Sampling Turbulence in the Stratified Ocean: Statistical Consequences of Strong Intermittency

MARK A. BAKER*

Scripps Institution of Oceanography, University of California at San Diego, La Jolla, CA 92093

CARL H. GIBSON

Departments of Applied Mechanics and Engineering Sciences and Scripps Institution of Oceanography, University of California at San Diego, La Jolla, CA 92093

(Manuscript received 6 May 1985, in final form 4 August 1986)

ABSTRACT

Turbulence and turbulent mixing in the ocean are strongly intermittent in amplitude, space and time. The degree of intermittency is measured by the "intermittency factor" σ^2, defined as either $\sigma^2_{\ln\epsilon}$, the variance of the logarithm of the viscous dissipation rate ϵ, or $\sigma^2_{\ln\chi}$, the variance of the logarithm of the temperature dissipation rate χ. Available data suggest that the cumulative distribution functions of ϵ and χ in stratified layers are approximately lognormal with large σ^2 values in the range 3–7. Departures from lognormality are remarkably similar to those for Monte Carlo generated lognormal distributions contaminated with simulated noise and undersampling effects.

Confidence limits for the maximum likelihood estimator of the mean of a lognormal random variable are determined by Monte Carlo techniques and by theoretical modeling. They show that such large σ^2 values cause large uncertainty in estimates of the mean unless the number of data samples is extremely large. To obtain estimates of mean dissipation rates $\bar{\epsilon}$ and $\bar{\chi}$ with ±10% accuracy at the 95% confidence level in the seasonal thermocline, the main thermocline or Pacific equatorial undercurrent (all stratified layers with large intermittency) requires 2600 or 10 000 independent data samples for $\sigma^2 = 3$ or 7, respectively.

If intermittency is ignored and the data are treated as if normally distributed, mean dissipation rates will probably be underestimated from a small number of samples. For example, it is generally accepted that canonical estimates of the main thermocline vertical eddy diffusivity of order 1 cm^2 s^{-1}, based on bulk property models, are inconsistent with much smaller values inferred, ignoring intermittency effects, from thermocline microstructure measurements. However, after accounting for the intermittent lognormality of the data, no statistically significant discrepancy exists.

Intermittency may cause qualitative as well as quantitative undersampling errors: minimum values in the vertical profiles of mean dissipation rates are commonly inferred from individual profiles at the seasonal thermocline depth and the equatorial undercurrent high-velocity core depth where maxima may actually exist. From the new confidence intervals, such minima are shown to be artifacts of the extreme intermittency in these strongly stratified layers.

1. Introduction

Viscous and diffusive dissipation rates ϵ and χ of turbulent velocity and temperature fluctuations in the ocean are enormously intermittent in magnitude, space and time, where $\epsilon = 2\nu e_{ij}^2$, $e_{ij} = (u_{i,j} + u_{j,i})/2$, $\chi = 2D(T_{,i})^2$, ν is the kinematic viscosity, D is the thermal diffusivity, $\mathbf{u}$ is the velocity, T is the temperature, and commas denote partial differentiation with respect to the spatial coordinates $\mathbf{x}$ with indices $i,j = 1, 2$ or 3. Repeated indices are summed.

The range of local values in a given layer may be five orders of magnitude in ϵ and ten orders of magnitude in χ. Space averages may be intermittent in time, and time averages intermittent in space. Even the intermittency may be intermittent because adjacent layers may have different mechanisms which govern their turbulence and mixing. Accurate estimates of mean dissipation rates and other turbulence and mixing parameters such as the Cox number $C \equiv (T_{,i}^2)/(\overline{T}_{,i})^2$, and the (microstructure) vertical eddy diffusivity $K_\rho \equiv D\overline{C}$, must take these various classes of intermittency into account. The present paper focuses on the statistical consequences of intermittency in sampling ocean turbulence and mixing. The hydrodynamic implications of the intermittency are discussed by Gibson (1980, 1981, 1982a,b,c, 1983, 1986, 1987a,b).

Gregg et al. (1973), Williams (1974), Belyaev et al. (1975a), Osborn (1978), Elliott and Oakey (1979), Gregg (1980), Crawford (1982), Washburn and Gibson (1984), Osborn and Lueck (1985) and Oakey (1985) all find oceanic turbulence dissipation parameters $X \equiv C$, χ and ϵ to be approximately lognormal. Typical microstructure datasets consist of only 10–100 samples.

* Present affiliation: The Johns Hopkins University Applied Physics Laboratory, Laurel, MD 20707.

Arithmetic means, modes and medians of such small datasets are satisfactory estimators of expected values $\bar{X}$ for normally distributed random variables (Nrvs), but generally result in severe underestimates of $\bar{X}$ for intermittent lognormally distributed random variables (LNrvs) such as ϵ and χ in the stratified ocean. The juxtaposition of "intermittent" and "lognormal" is intended to identify lognormal random variables with large "intermittency factors" $\sigma^2_{\ln X}$. "Large" is defined by the threshold $\sigma^2_{\ln X}$ greater than 3 which yields mean-to-mode ratios for LNrvs greater than order 100. "Intermittent lognormality" is not intended to imply on/off lognormality nor should it be interpreted to mean that the variable is discrete rather than continuous. It does imply that the dominant contribution to the expected value is produced by a small fraction of the volume sampled.

The sampling problems induced by intermittency have been known for many years in atmospheric turbulence studies. Gibson et al. (1970) report intermittency factors $\sigma^2_{\ln\epsilon}$ as large as 4.0 in the marine atmospheric boundary layer, and good agreement with the lognormal distribution for ϵ proposed by Kolmogoroff (1962), discussed in section 5. Tennekes and Wyngaard (1972) warn that such extreme intermittency of small-scale turbulence imposes significant data processing hazards, both in signal-to-noise and time integration, for estimating average values with acceptable accuracy. They refer to kurtosis values of velocity derivatives in the atmosphere over land of about 40, corresponding to $\sigma^2_{\ln\epsilon}$ values of about 3.7 assuming lognormality. In contrast, Hald (1952), in his review of lognormal distributions, presents an example of a lognormal distribution he describes as "markedly skew" although the $\sigma^2_{\ln\chi}$ value is only 1.1. Such small values of $\sigma^2_{\ln\epsilon}$ and $\sigma^2_{\ln\chi}$, in the range 1–2, have only been observed in the surface mixed layer and other strong shear layers in the ocean. Gibson (1983) shows $\sigma^2_{\ln\chi}$ is in the range 0.5–1.5 for the mixed layer data of Dillon (1982); Osborn and Lueck (1985) derive a $\sigma^2_{\ln\epsilon}$ value of 1.96 from measurements of velocity fluctuations in the surface mixed layer; and in section 4a a value of $\sigma^2_{\ln\epsilon} = 0.62$ is derived for the strong shear layer above the equatorial undercurrent from the data of Crawford (1982).

The properties of lognormal random variables are detailed in appendix A. Briefly, the expected value, $E(X)$, of a lognormal random variable X is given by $\exp(\mu + \sigma^2/2)$, where μ is the expected value and σ^2 is the variance of the Gaussian random variable $Y = \ln X$. The maximum likelihood estimator of $E(X)$ is $\bar{X}_{\text{mle}} = \exp(m + s^2/2)$, where m and s^2 are the arithmetic sample mean and variance of Y, respectively. The use of lognormal probability plots to estimate μ and σ^2 is outlined. In appendix B the rationale for selecting $\bar{X}_{\text{mle}}$ to estimate $E(X)$ is derived. In particular, the arithmetic mean, $\bar{X}_{\text{am}}$, is shown to require significantly more samples than required by $\bar{X}_{\text{mle}}$ for the same degree of statistical uncertainty when the intermittency factor $\sigma^2_{\ln X}$ is large. Readers are strongly encouraged to review appendices A and B, *which are of a tutorial nature* and form the statistical basis of the present paper.

In section 2, empirical oceanic cumulative distribution functions (CDFs) and their observed departures from lognormality are compared to CDFs generated by Monte Carlo methods, which include simulated noise. A specific procedure to estimate μ and σ^2 and the degree of noise contamination in the measured CDFs is given. Section 3 examines confidence intervals used by Elliott and Oakey (1979, 1980) and Oakey (1985) to indicate the uncertainty in their $\bar{X}_{\text{mle}}$ estimates of $E(X)$. Their intervals will be shown to be incorrect. New confidence intervals are derived theoretically and are tested by comparison to intervals generated by Monte Carlo methods. These new theoretical intervals are strongly dependent on the intermittency parameter $\sigma^2_{\ln X}$, and allow estimation of the necessary number of samples required to estimate the expected value at a given level of uncertainty.

In section 4 several microstructure datasets from the Atlantic and Pacific equatorial undercurrents, the seasonal thermocline and the main thermocline are reviewed to test the validity and consequences of the hypothesis of lognormality. The results are discussed in section 5, and conclusions are presented in section 6.

2. Noise and sample size effects on the CDF

A result common to many of the oceanic empirical CDFs is the apparent departure from lognormality of the upper and lower tails of the CDFs. Given an extremely large sample of a LNrv and an ideal measurement system, without noise or sensor limitations, the measured random variable would be lognormal, the empirical CDF would fit a straight line on a lognormal probability plot and would pass any number of statistical tests for lognormality. Unfortunately, noise is always present in microstructure measurements along with sensor limitations and limited sample size.

The separate effects of noise and sample size on the empirical CDF may be demonstrated by Monte Carlo methods. A first-order model of the measured signal S is

$$S_{\text{meas}}(t) = [h(t)^* S_{\text{true}}(t) + n(t)]^* g(t) \qquad (1)$$

where $h(t)$ is the impulse response function corresponding to frequency or spatial response limitations, the asterisk denotes convolution, $n(t)$ is the noise portion of the signal, and $g(t)$ represents the impulse response function of the filter(s) used.

For microstructure measurements, $S_{\text{meas}}(t)$ might represent conductivity, temperature or vertical shear of the horizontal velocity. Dissipation rates χ and ϵ may be computed by integrating the temperature gradient spectrum and the vertical shear of horizontal velocity spectrum, respectively, assuming isotropy and using the Taylor hypothesis $f = Uk/2\pi$. The variances

of different wavenumber, k, bands are computed and integrated over the wavenumber bands of interest. This results in estimates of the band-passed signal variance for that segment of the data record.

Noise measurements for conductivity, temperature or vertical shear of the horizontal velocity indicate approximately bandlimited white noise for these signals. Figure 5 of Gregg and Pederson (1980) displays conductivity spectra which have the characteristic flatness indicative of bandlimited white noise in the dissipation wavenumber band. Figure 6 of Crawford and Osborn (1980) shows the noise spectrum for the velocity shear probe is also relatively flat in the wavenumber band used to estimate ϵ. Figure 5 of Oakey (1982) shows noise spectra in terms of temperature gradient spectra which have approximately +2 slopes indicating a bandlimited white noise spectrum for the temperature signal.

It should be emphasized in this discussion that it is not critical that the empirical noise distributions be exactly bandlimited white noise. What is necessary is the realization that the presence of noise, or attempts to subtract noise from signals, will result in departures of the measured distribution function from the underlying true signal distribution function. Note that if the data come from a particularly active region, or if the averaging length is long enough so that significant signal variance is measured, the effect of noise on the measured distribution is reduced.

The noise contributes a variable percentage of the measured variance, depending on signal strength. Noise levels are generally estimated by examining the quietest portions of the data records and are usually quoted in terms of equivalent $°C^2\ s^{-1}$ and $cm^2\ s^{-3}$ for χ and ϵ, respectively. To attempt to reproduce the effect that noise has on empirical CDFs, the following procedure is employed. Gaussian random numbers Z_i are generated that are distributed as $N(0, \sigma_n)$, where σ_n^2 is the quoted equivalent noise variance in the measured oceanic signal. A new random variable

$$Y_n = \frac{1}{n-1}\sum_{i=1}^{n}(Z_i - \bar{Z})^2 \qquad (2)$$

is formed that has an expected value of σ_n^2 and variance $2\sigma_n^4/(n-1)$, where

$$\bar{Z} = \frac{1}{n}\sum_{i=1}^{n} Z_i. \qquad (3)$$

The sample size n is chosen to be about 10–20 due to the recognized variability in the estimated oceanic noise levels. Oakey (1982), for instance, cites an uncertainty of a factor of 2 in the quoted noise variance. Lognormal random variables are generated using the same sample sizes and graphically estimated statistics from the measured oceanic datasets. The noise samples Y_n are added to these lognormal random variables to simulate the presence of noise. If noise subtraction is performed in the measured oceanic data, a constant noise factor of σ_n^2 is then subtracted to mimic crudely the procedures employed. Lognormal probability plots of these Monte Carlo runs are generated for comparison to the empirical oceanic data.

Figures 1, 2 and 3 are Monte Carlo simulations, using the procedure outlined above, of lognormal probability plots of the oceanic datasets from section 4 shown in Figs. 7c, 8 and 10. In each case, the statistics of the oceanic dataset, shown by the straight line in Figs. 1, 2 and 3, are used to seed the lognormal random number generator and the noise variance is used to seed the Gaussian random number generator. The noise levels used for Figs. 1, 2 and 3 are $4 \times 10^{-6}\ cm^2\ s^{-3}$, $2.4 \times 10^{-7}\ °C^2\ s^{-1}$ and $1.3 \times 10^{-8}\ °C^2\ s^{-1}$, respectively. These values can be found in Crawford and Osborn (1980), Washburn and Gibson (1984) and Oakey (1982), respectively. The n for the Y_n computations are 8, 15 and 20, respectively. In Figs. 2 and 3, a constant noise factor, equal to the respective value cited above, is subtracted after addition of the random noise to approximate the noise subtraction methods used in the oceanic examples. Noise subtraction in the measured data is performed by integrating the difference between the signal spectrum and the noise spectrum until the difference is zero or negative.

In each case the essential characteristics of the oceanic CDFs are reproduced. The straight line shown

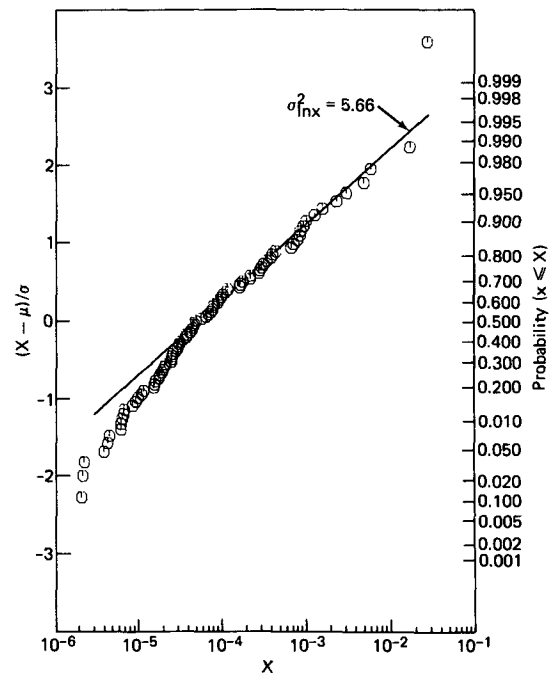

FIG. 1. Lognormal probability plot of a lognormal random variable contaminated with simulated noise effects. Signal and noise statistics correspond to the below-core region of the equatorial undercurrent data of Crawford (1976), shown in Fig. 7c. The straight line corresponds to the signal statistics produced by the graphical fit shown in Fig. 7c. Note the similarity in CDF shapes for Figs. 1 and 7c.

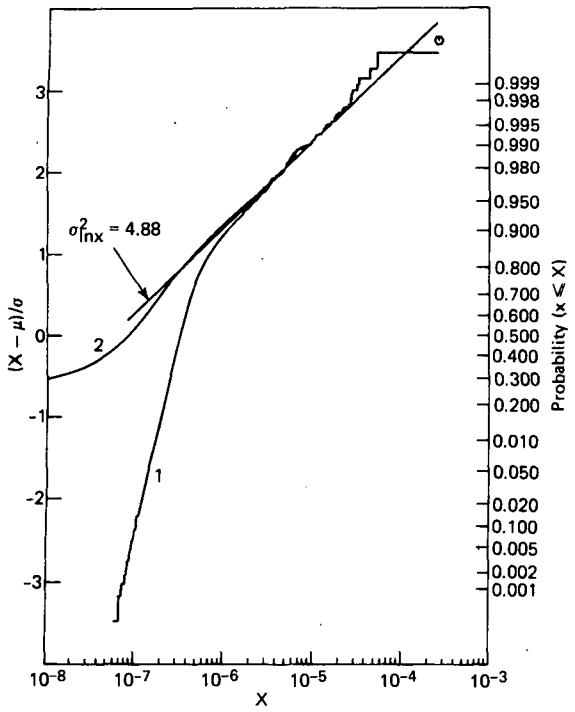

FIG. 2. Curve 1 is based on the same procedure employed in Fig. 1, using the signal and noise statistics corresponding to data of Fig. 8 from the seasonal thermocline data of Washburn and Gibson (1984). Curve 2 represents the data from curve 1 corrected for noise by subtracting a noise constant and corresponds to curve 2 in Fig. 8. The straight line corresponds to the signal statistics produced by the graphical fit shown in Fig. 8.

in each simulation corresponds to the signal statistics estimated from the oceanic datasets using the graphic procedure. When noise subtraction is not performed, the CDFs droop at the low end. When noise subtraction is employed, the CDFs break up and away from the true underlying lognormal distribution. The appearance of the upper and lower tails of the Monte Carlo CDFs are remarkably similar to the oceanic examples. In the Monte Carlo runs the apparent deviation from the underlying distribution in the upper tail is attributed to sample size, rather than to any underlying departure from lognormality or as a consequence of sensor resolution limitations.

Samples may be encountered with significant variance at scales beyond the resolution of the sensor. These unresolved samples are falsely measured as smaller values. The upper tail of the empirical CDF will then break up and away from the true underlying distribution falsely indicating a deficit of larger values.

The Monte Carlo runs fail statistical tests such as the χ^2 goodness-of-fit test for lognormality just as badly as the oceanic examples. For cases where noise contamination is a problem it would be more appropriate to apply such tests assuming the measured random variable is the sum of a lognormal random variable and a noise random variable. Careful statistical studies of the time series and the resultant processing would allow a more accurate characterization of the CDF of the noise portion of the final product of the data analysis. Assuming the noise is independent of the signal, goodness-of-fit tests would be applied to the probability density function, pdf, resulting from the sum of the signal and noise random variables. Application of χ^2 tests without accounting for the presence of noise will generally fail, but the conclusion that the underlying distribution is significantly different from lognormal is then questionable.

Assume the noise variance, random variable X_1, is independent of the signal variance, random variable X_2. Note both are positively distributed random variables. The cumulative distribution function CDF(y) of the random variable $Y = X_1 + X_2$ is given by

$$\mathrm{CDF}(y) = \int_0^y \int_0^{y'} f_1(x_1) f_2(y' - x_1) dx_1 dy' \qquad (4)$$

from Hoel et al. (1971), where f_1 and f_2 are the probability density functions of X_1 and X_2, respectively. The inner integral is a convolution of the two density functions and indicates the possibility of contamination of the true signal CDF over an interval rather than the noise inducing only a simple cutoff of the CDF. The excellent agreement between the simulated and measured distributions implies that the measured distributions are derived from a convolution of approximately Gaussian noise distributions with underlying lognormal distributions.

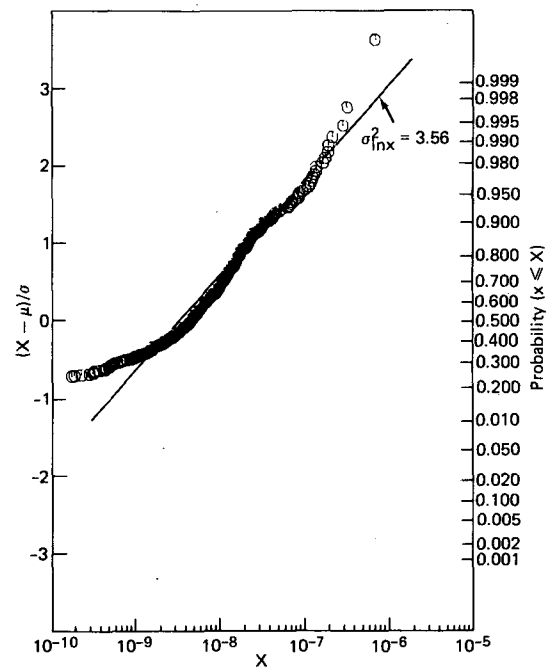

FIG. 3. As in Fig. 1 except with noise subtraction, corresponding to Fig. 10 for the subseasonal thermocline data of Elliott and Oakey (1979), which also were corrected by noise subtraction. The straight line corresponds to the signal statistics produced by the graphical fit shown in Fig. 10.

Based on the Monte Carlo runs and the above results, the following procedure is recommended for determination of the degree of noise contamination, and for estimating μ and σ^2 if the contamination is excessive. Two sample sets should be generated for each comparison to lognormality of ϵ or χ on a probability plot. A noise spectrum ϕ_n should be estimated from a quiet section of the record. The first sample set may be generated by integrating the measured spectrum ϕ_m over a fixed frequency range. An alternative procedure for this sample set is to integrate ϕ_m until it intersects ϕ_n. Both procedures will *still* include noise over the band of integration. Note that if m and s^2 are computed from sample sets derived from both of these procedures, method 2 will produce closer estimates of the true values than method 1. The second sample set from the same data record is generated by integrating $(\phi_m - \phi_n)$ until the difference is zero or negative.

Both sample sets are then plotted on lognormal probability paper. Where the two curves converge and the linear range begins indicates the start of the resolved portion of the CDF. A least-square line should be fitted to this linear range and μ and σ^2 estimated as described in appendix A. Washburn and Gibson (1984) employ the procedure outlined above, except the estimates are generated by a visual fit to the linear region.

If the signal is always appreciably above the noise, or if σ^2 is small, there will be little difference between these graphical estimates of μ and σ^2 and the arithmetic estimates m and s^2. In those cases, the arithmetic estimates are preferred. But in cases where the indicated noise contamination is excessive (>20%) and for an underlying $\sigma^2 > 3$, the graphical procedure is more accurate.

For example, m is -14.76 and s^2 is 0.72 for the data corresponding to curve 1 in Fig. 2, but the true values of μ and σ^2 are -16.74 and 4.88, respectively. The graphical procedure yields the estimates -16.73 and 4.73 for μ and σ^2, respectively. For such noise contaminated data, μ will be overestimated and σ^2 underestimated by m and s^2, respectively. In addition, the difference $(\sigma^2_{\text{true}} - s^2)$ increases as the noise contamination increases.

Because the underlying distribution in the modeled signal is lognormal and the simulations of noise and limited sample size appear reasonable, the striking similarity of the deviations from lognormality of both oceanic and modeled datasets suggests that much of the deviation of the oceanic distributions from lognormality is due to noise and sample size effects. The conclusion is that deviations from lognormality observed so far in the oceanic data cannot be taken as evidence against lognormality of the underlying distributions.

3. Confidence intervals for $\bar{X}_{\text{mle}}$

Elliott and Oakey (1979) find that the Cox number is approximately lognormally distributed for their data. In Elliott and Oakey (1979, 1980), $\bar{X}_{\text{mle}}$ is used to estimate the expected value of the microstructure parameters and in both papers confidence intervals for the estimate of the expected value are employed. These are the first published attempts by oceanic microstructure investigators to construct confidence limits for the expected value of an LNrv estimated by $\bar{X}_{\text{mle}}$. In Elliott and Oakey (1979), the explicit form of the confidence intervals is not presented, but on page 288 they state:

> From the characteristic of log-normality, some estimate can be made for the confidence interval for the means. Using the mean value of the Cox number and standard deviation of the plot in Fig. 5 ($\ln\sigma = 1.8$) as representative for individual segments with 37 samples, then, when transformed into linear coordinates (Hald, 1952), the 95% confidence limits become $2.24 < \bar{C} \approx 4 < 7.75$. Thus for our data, the mean values for each 10 m segment (0–1, 1–2, . . . , 8–9) should be accurate (95% confidence limits) to within a factor of 2.

In Elliott and Oakey (1980), $\bar{X}_{\text{mle}}$ is employed to estimate the mean Cox number. In addition, Elliott and Oakey (1980) state:

> As was described in Hald (1952), we have calculated log ξ = mean(log$x$) and σ^2 = Var(log$x$) and from these have obtained the median(x) = ξ and the mean(x) = $\xi \times 10^{\sigma^2/2 \log_{10} e}$, where the 1σ confidence limits are given by $\xi/10^{\sigma} < \bar{X} < \xi \times 10^{\sigma}$.

In the notation of the present paper, $\xi = \exp(m)$, $\bar{X} = \bar{X}_{\text{mle}}$ and $\sigma = s$. The method of calculation of ξ, σ and the median and mean are correct for a lognormal distribution. However, note the lack of sample size dependence. These "confidence limits" actually represent the $(\alpha/2)$ and the $(1 - \alpha/2)$ percentile points for a theoretical (not empirical) distribution assuming that μ and σ are *known*, not estimates. They indicate the skewness of the distribution of X and are not presented as confidence intervals by Hald. Oakey (1985) modifies these intervals by incorporating sample size. The new intervals are given by

$$\xi \times 10^{-z_{\alpha/2}\sigma n^{-1/2}} < \text{mean}(X) < \xi \times 10^{z_{\alpha/2}\sigma n^{-1/2}} \qquad (5)$$

where the $z_{\alpha/2}$ is based on the degree of confidence. Oakey used $z_{\alpha/2} = 0.98$, or a 68% confidence interval. The new limits have two correct interpretations. They are the *empirical* percentile points of the empirical distribution, and they are also the correct confidence intervals for the *median* of X. They are *not* the correct confidence intervals for the expected value of X, based on using $\bar{X}_{\text{mle}}$.

Confidence intervals may be formed based on $\bar{X}_{\text{mle}}$ from the Gaussian properties of the estimators m and s^2. These intervals are approximately correct for very small samples and become increasingly accurate with increasing sample size. Because m is the arithmetic mean of Nrvs, it is $N(\mu, \sigma n^{-1/2})$. The arithmetic sample variance, s^2, is asymptotically $N[\sigma^2, \sqrt{2}\sigma^2(n-1)^{-1/2}]$, from Cramer (1946). The distribution of s^2 is well rep-

resented by the Gaussian distribution for $n > 30$. For Nrvs, m and s^2 are independent random variables. Therefore, the sum $S = m + s^2/2$ is a random variable that is asymptotically $N\{\mu + \sigma^2/2, [\sigma^2/n + \sigma^4/2(n - 1)]^{1/2}\}$. The new random variable S is standardized, yielding

$$Z = \frac{(m + s^2/2) - (\mu + \sigma^2/2)}{[\sigma^2/n + \sigma^4/2(n-1)]^{1/2}} \quad (6)$$

which is asymptotically $N(0, 1)$. Confidence intervals for Z are now easily formed. Rearrangement of terms and then transformation of the intervals by the exp operation lead to the following confidence intervals based on $\bar{X}_{\text{mle}}$ of LNrvs:

$$\bar{X}_{\text{mle}} \exp(-\eta z_{\alpha/2}) < E(X) < \bar{X}_{\text{mle}} \exp(\eta z_{\alpha/2}) \quad (7)$$

with a $(1 - \alpha)$ confidence coefficient, where $\eta = [\sigma^2/n + \sigma^4/2(n - 1)]^{1/2}$. Because $\bar{X}_{\text{mle}}$ equals $\exp(S)$, from (B9), and S is approximately normal, $\bar{X}_{\text{mle}}$ should be approximately lognormally distributed. Asymptotical normality is a property of maximum likelihood estimators, and implies the lognormal distribution of $\bar{X}_{\text{mle}}$ should converge to a normal distribution as $n \to \infty$.

Using a Gaussian random number generator, 40 000 random numbers that are $N(2.98, \sqrt{4.41})$ are generated. The values of μ and σ^2 correspond to the arithmetic estimates of $\mu_{\ln C}$ and $\sigma^2_{\ln C}$ for the Gregg (1977) data (see Table 1). From these 40 000 random numbers, two sets of 4000 estimates of $\bar{X}_{\text{mle}}$, using the arithmetic and graphical methods, are formed from subsets of size 10. Shown in Fig. 4a are the normal (curve 1) and lognormal (curve 2) probability plots for the 4000 estimates produced by the arithmetic method. The lognormal (curve 3) probability plot for the 4000 estimates yielded by the graphical procedure is also displayed. Figure 4a indicates $\bar{X}_{\text{mle}}$ is clearly non-Gaussian and is approximately lognormal for $n = 10$. The straight line is the expected CDF, $N(5.185, \sqrt{1.52})$, if the sum $(m + s^2/2)$ is Gaussian for $n = 10$. The arithmetic mean and variance of the 4000 arithmetic estimates of $(\mu + \sigma^2/2)$ are 5.168 and 1.47, respectively, which compare quite well with the expected values. The arithmetic mean and variance of the 4000 graphical estimates of $(\mu + \sigma^2/2)$ are 5.31 and 2.38, respectively. Also shown in Fig. 4a are the 0.05 and 0.95 percentile points for the empirical CDF (curve 2) generated by the arithmetic method. These percentile points correspond to a realization of the 90% confidence interval for $\bar{X}_{\text{mle}}$. The 90% confidence interval, (24, 1358), generated by Eq. (7), compares quite well with the Monte Carlo interval, (29, 1396), displayed in Fig. 4a. Intervals derived from (7) also agree, for large samples, with the large sample intervals presented in appendix B, Eq. (B15).

A closer look at Fig. 4a reveals that for large $\sigma^2_{\ln X}$, small n, and significance levels in the range 95% to 99%, both upper and lower confidence limits generated by (7) are underestimates. This should be kept in mind

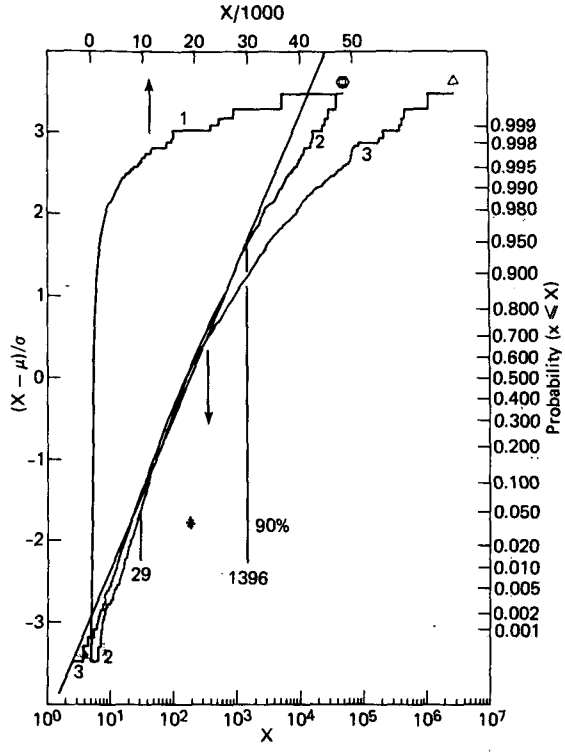

FIG. 4a. Lognormal (2) and normal (1) probability plots for Monte Carlo generated values of the estimator $\bar{X}_{\text{mle}}$, based on the arithmetic method. Parameters $N = 10$, $\mu = 2.98$ and $\sigma^2 = 4.41$ are approximately equal to those for the Gregg (1977) $\bar{C}_{150\text{ m}}$ measurements, shown in Fig. 14. The straight line is the theoretical lognormal CDF of $\bar{X}_{\text{mle}}$ based on the assumption $m + s^2/2$ is normally distributed, for $N = 10$.

in section 4 where, generally, the limits are quite wide. Because the exact probability distributions of m and s^2 are known, new tables could be generated and exact intervals obtained since the CDF of the sum of two independent random variables result from the convolution of the individual pdfs. Such tables would have to cover a wide range in m, s^2 and n. However, because the number of samples required for a statistically significant estimate is shown to be quite large, this should be unnecessary.

Figure 4b shows lognormal probability plots of $\bar{X}_{\text{mle}}$ estimated by the arithmetic method, curve 1, and the graphical method outlined in appendix A (curve 2) for $n = 100$ and the same μ and σ^2 as in Fig. 4a. The theoretical CDF, $N(5.185, \sqrt{0.142})$, of $\ln(\bar{X}_{\text{mle}})$, based on the properties of m and s^2, is again shown by the straight line. The fit of the $\bar{X}_{\text{mle}}$ estimates generated by the arithmetic method is extended to the 0.99 and 0.01 percentiles of the theoretical CDF before departures start to occur. The arithmetic mean and variance of the 4000 samples of $(m + s^2/2)$ are 5.180 and 0.142, respectively, which again compare quite well with the expected values. The empirical CDFs produced by the arithmetic and graphical procedures are virtually in-

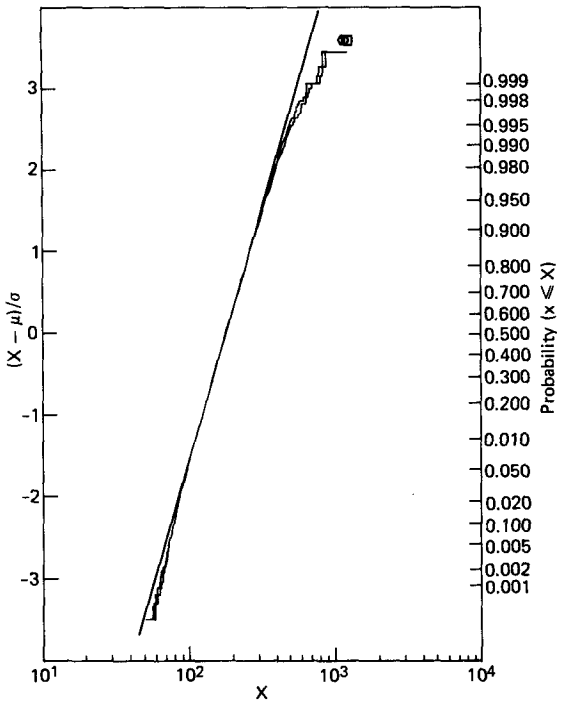

FIG. 4b. Lognormal probability plots for Monte Carlo generated values of $\bar{X}_{\text{mle}}$ based on the arithmetic method and the graphical method of estimating the parameters μ and σ^2. $N = 100$, $\mu = 2.98$ and $\sigma^2 = 4.41$. The straight line is again the theoretical CDF, but for $N = 100$.

distinguishable for $n = 100$. Note: a $<$ sorting procedure rather than the $\leqslant$ sorting procedure actually used, would introduce a positive bias in the graphical estimates. The arithmetic mean and variance of the 4000 graphical estimates of $(\mu + \sigma^2/2)$ are 5.184 and 0.148, respectively.

Although theoretical confidence intervals are not available for the graphical technique, the graphical method has the advantage that it needs only to resolve a portion of the CDF accurately in order to make an accurate estimate of the parameters of the distribution. Inclusion of excessively noise-contaminated data results in underestimates of $\sigma^2_{\ln X}$ using the arithmetic method. When the fraction of the samples at or below the noise level is excessive, confidence intervals are constructed using (7) and the graphical estimates of $\mu_{\ln X}$ and $\sigma^2_{\ln X}$.

Figure 4b indicates that for sample sizes of $\sim$100 or larger the confidence limits generated by such graphical replacements are relatively accurate. The three cases in this paper where the noise contamination is excessive have sample sizes of 84, 333 and 3792 and σ^2 values of 5.91, 3.56 and 4.88, respectively. Figure 4b indicates that insertion of these graphical estimates into (7) is reasonable and justified.

As shown in Fig. 4a, for small samples of size about 10 and large σ^2 about 5, the CDF of graphical estimates begins to depart significantly from the predicted line based on the arithmetic method with corresponding distortions of confidence intervals estimated from (7).

Using (7), the number of independent samples necessary to obtain an estimate of the expected value within $\pm\delta$ of the true value, at a desired significance level, may be calculated. Figure 5 shows the number of independent samples required for various values of $-\delta$ at the 95% significance level. If the -1 is neglected in the term $\sigma^4/2(n-1)$, the number of independent samples required for a given δ is

$$n \approx \frac{(\sigma^2 + \sigma^4/2)(z_{\alpha/2})^2}{[\ln(1 \pm \delta)]^2} \tag{8}$$

Assuming σ^2 is in the range 3–7, Fig. 5 shows that a range of 2600 to 10 000 independent samples is required, respectively, for estimating the expected value to 10% accuracy with 95% confidence using $\bar{X}_{\text{mle}}$.

The approximate number of samples required for $\bar{X}_{\text{am}}$ to obtain an estimate of the expected value within $\pm\delta$ is computed by combining the relative efficiency of $\bar{X}_{\text{am}}$ from the ratio of (B13) to (B10) and the number of samples required for $\bar{X}_{\text{mle}}$ to obtain the same degree of accuracy. This is shown in Fig. 6 for $-\delta$. Whereas $\bar{X}_{\text{mle}}$ requires 2600 to 10 000 samples for 10% accuracy at the 95% level for σ^2 in the range of 3–7, $\bar{X}_{\text{am}}$ requires 7000 to 400 000 samples: an increase by factors of 3 to 40.

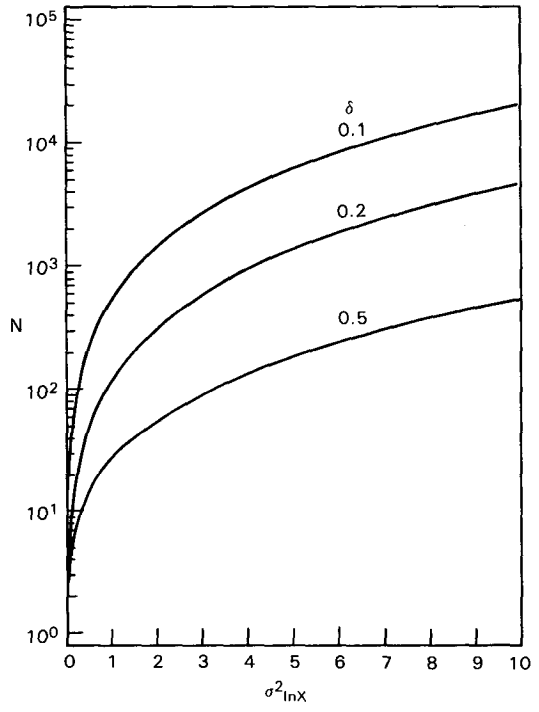

FIG. 5. The number of independent samples N required to estimate the expected value of a LNrv within $-\delta$ of the true value at the 95% significance level using the maximum likelihood estimator $\bar{X}_{\text{mle}}$, from (8).

4. Reexamination of oceanic microstructure datasets

Figures 7–10 and 14 show lognormal probability plots of several oceanic microstructure datasets in the equatorial undercurrent, seasonal thermocline and main thermocline layers. These datasets are reviewed to test the hypothesis of lognormality of oceanic turbulence and mixing parameters and to reinterpret various estimates of mean values taking the intermittency of the data into account.

The CDFs of oceanic mixing parameters will be difficult to resolve fully. The low end of the CDF is distorted by noise contamination of the smallest measured values. Inadequate spatial or frequency response and inadequate sample size cause distortion of the high end. The dependence of the estimated expected value $\hat{E}(X)$ on the unresolved tail regions of the sample CDF may be readily ascertained. The fraction $F(x)$ of $\hat{E}(X)$ contributed by values less than x is given by

$$F_i(x) = \int_0^x \frac{\exp[-(\ln X - \hat{\mu})^2/2\hat{\sigma}^2]dX}{\hat{\sigma}\sqrt{2\pi}\exp(\hat{\mu} + \hat{\sigma}^2/2)} \qquad (9)$$

where ^ indicates estimates. $F_i(x)$ is evaluated based on either the arithmetic, $i = 1$, or the graphical, $i = 2$, estimates of $\mu_{\ln X}$ and $\sigma^2_{\ln X}$ for each comparison to lognormal in Figs. 7–10, 14. The + indicates the largest value of the dataset. Also shown in each comparison to lognormal are the 95% confidence intervals for the expected value based on the indicated value of $\bar{X}_{\text{mle}}$. The subscript associated with $\bar{X}_{\text{mle}}$ indicates that the estimate is produced by the arithmetic, 1, or graphical, 2, methods. The value of $\bar{X}_{\text{mle}}$ is indicated by an asterisk. The statistical summary is presented in Table 1.

a. *Equatorial undercurrents*

Measurements of velocity and temperature microstructure in the Pacific equatorial region at 150°W are presented by Crawford (1982). Crawford shows a fit to lognormal of 20 m average $\bar{\epsilon}$ values, computed for the depth range 40–120 m, and a vertical heat flux parameter K_H, computed for depths 60–120 m. Crawford finds the lognormal fits to be excellent, as long as values are restricted to within ±0.5° of the equator, corresponding to 19 drops within this category. Crawford goes on to state that:

> The standard deviations for the lognormal distributions of $\bar{\epsilon}$ and K_H are 1.0 and 1.1, respectively, smaller than the value of 1.8 for K_H observed by Elliott and Oakey in the thermocline at 9°N, 22°W. One expects internal

TABLE 1. Statistical summary of the reexamined oceanic microstructure datasets.

Depth	$\bar{X}am$	$\bar{X}mle_1$	$\bar{X}mle_2$	μ_1/μ_2	σ_1^2/σ_2^2	R_1/R_2 [4]	N	Confidence interval (95%)
Equatorial undercurrent								
Crawford and Osborn (1981) $\epsilon(cm^2/sec^3)$ 30'S - 15'N 150°W								
40-60 *m*	1.2×10^{-3}	1.7×10^{-3}	2×10^{-3}	-7.25/-7.46	1.68/2.5	12/43	9	$5\times10^{-4} < \bar{\epsilon} < 5\times10^{-3}$
60-80 *m*	9.2×10^{-4}	9.7×10^{-4}	9.4×10^{-4}	-7.25/-7.39	0.62/0.85	2.5/3.6	9	$5\times10^{-4} < \bar{\epsilon} < 1.8\times10^{-3}$
80-100 *m*	8.5×10^{-4}	1.1×10^{-3}	9.1×10^{-4}	-8.26/-8.61	2.91/3.22	79/125	9	$1.8\times10^{-4} < \bar{\epsilon} < 6.8\times10^{-3}$
100-120 *m*	1.1×10^{-3}	4.3×10^{-3}	9.7×10^{-3}	-9.15/-9.63	7.39/9.99	$65186/3.2\times10^6$	9	$8\times10^{-5} < \bar{\epsilon} < 2\times10^{-1}$
Crawford (1976) ϵ (cm^2/sec^3) 18'S - 37'N 24-33° W								
Above core	3.6×10^{-3}	6.5×10^{-3}	8.8×10^{-3}	-6.74/-6.73	3.4/4.0	164/403	82	$3.3\times10^{-3} < \bar{\epsilon} < 1.27\times10^{-2}$
Core	1.0×10^{-4}	**	1.1×10^{-4}	**/-12.05	**/5.91	**/7080	84	$4.0\times10^{-5} < \bar{\epsilon} < 3.2\times10^{-4}$ *
Below core	5.6×10^{-4}	4.8×10^{-4}	8.6×10^{-4}	-9.4/-9.89	3.5/5.66	191/4866	84	$3.16\times10^{-4} < \bar{\epsilon} < 2.3\times10^{-3}$ *
Seasonal thermocline								
Washburn and Gibson (1984) $\chi(°C^2/sec)$ 50°N 145°W								
≈ 37 *m*	0.84/1.05 $\times10^{-6}$ [3]	**	6.2×10^{-7}	**/-16.74	**/4.88	**/1510	3792	$5.4\times10^{-7} < \bar{\chi} < 7\times10^{-7}$ *
Dillon (1982) $\chi(°C^2/sec)$ 50°N 145°W								
30-40 *m*	7.3×10^{-5}	2.6×10^{-4}	4.6×10^{-4}	-11.5/-11.66	6.49/7.97	16898/155593	32	$4\times10^{-5} < \bar{\chi} < 1.6\times10^{-3}$
Elliott and Oakey (1979) $\chi(°C^2/sec)$ 9°02'N 22°38'W								
35-125 *m*	2.2×10^{-8}	**	2.1×10^{-8}	**/-19.48	**/3.56	**/209	333	$1.5\times10^{-8} < \bar{\chi} < 2.9\times10^{-8}$ *
Main thermocline								
Gregg (1977) Cox number 28°N 155°W								
≈ 600-1200 *m*	95	179	181	2.98/2.6	4.41/5.2	746/2441	10	$16 < \bar{C} < 2003$

[1] Denotes arithmetic estimation of μ and σ^2

[2] Denotes graphical estimation of μ and σ^2

[3] $\bar{X}am$ computed: with noise subtraction/without noise subtraction

[4] R = mean to mode ratio = exp ($3\sigma^2/2$)

*Based on graphical estimates of μ and σ^2

**Method not used due to noise effects

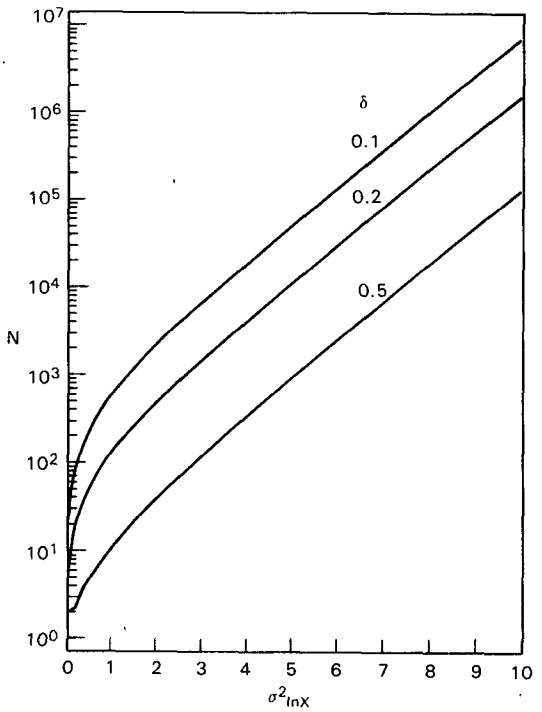

FIG. 6. As in Fig. 5 except the number of samples N is for the arithmetic mean $\bar{X}_{am}$ instead of the maximum likelihood estimator $\bar{X}_{mle}$, from (8) and the relative efficiency re = mse $(\bar{X}_{mle})/D^2(\bar{X}_{am})$. See Fig. B1.

> waves to contribute strongly to the shear at their position, while the zonal shear at the equator dominates the internal wave shear and maintains larger values of $\bar{\epsilon}$ at the equator. It could be that because the zonal shear varies over a smaller range than internal wave shear, the values of $\bar{\epsilon}$ and K_H will also vary less. If so, then *one can determine the nature of equatorial turbulence with fewer samples than are required in the seasonal thermocline at higher latitudes* (italics added). (p. 1147)

Actually, Crawford's data indicate a much larger rather than a smaller degree of intermittency than found by Elliott and Oakey (1979). This is because Crawford's estimates of the standard deviations of the logarithm of $\bar{\epsilon}$ and K_H are based on using *logarithms to the base 10,* whereas the Elliott and Oakey (1979) estimate is based on *logarithms to the base e.* Crawford's values of 1.0 and 1.1 become 2.3 and 2.54 when transformed to the standard system of base e employed by Elliott and Oakey. Therefore, $\sigma^2_{\ln X}$ values for Crawford's data become 5.3 and 6.4 for $\bar{\epsilon}$ and K_H, respectively. Corresponding mean-to-mode ratios R [see appendix A, (A7)] for $\bar{\epsilon}$ and K_H are 2836 and 14 765. The value of 14 765 should be compared to the Elliott and Oakey mean-to-mode ratio, based on their estimated value of $\sigma^2_{\ln C} = 3.24$, of only 129. Based on the measured CDFs, a *larger* rather than *smaller* number of samples will generally be required in equatorial regions than in thermocline layers at high latitudes to achieve the same accuracy in estimates of mean values.

A closer examination of the dataset is revealing. Figure 5a of Crawford (1982) shows 20 m, one-day, space–time averages of $\bar{\epsilon}$ from within ±0.5° of the equator, plotted in 20 m intervals of depth. The scatter of these $\bar{\epsilon}$ values at each depth range may be used to infer the vertical profile of the intermittency of the space–time average dissipation rate $\bar{\epsilon}_{\text{space-time}}$. The individual 20 m values from each profile are available in Table 5 of Crawford and Osborn (1981). Using the same space–time averaging as in Fig. 5a of Crawford (1982) and fitting data from each of the 20 m layers from 40–120 m to lognormal distributions indicates a great deal of variability in the intermittency.

Table 1 shows the resulting statistics. The intermittency factor $\sigma^2_{\ln\epsilon}$ ranges from 0.62 for the depth interval of 60–80 m to 7.39 for the 100–120 m interval. This is a range in mean-to-mode ratios of 2.5 to 65 186, demonstrating enormous variability in the intermittency of different layers in the Pacific equatorial undercurrent system.

Vibrational noise hypotheses have been proposed by Gregg (1976) and Crawford (1976, 1982) to explain the large discrepancies between their estimates of $\bar{\epsilon}$ and $\bar{\chi}$ and those of Williams and Gibson (1974) and Belyaev et al. (1975b) measured from towed bodies. Such hypotheses are inconsistent with direct measurements of the vibrational accelerations of the towed body by Schedvin (1979). The discrepancies are statistically insignificant because the confidence intervals of the $\bar{\epsilon}_{\text{mle}}$ and $\bar{\chi}_{\text{mle}}$ estimators overlap when intermittency is taken into account. Table 1 shows that for Crawford's Pacific data, the maximum dissipation occurs in the layer 100–120 m with an estimated mean value of $\bar{\epsilon}_{\text{mle}} = 4.3 \times 10^{-3}$ cm^2 s^{-3}. The 95% confidence interval is $7.6 \times 10^{-5} < \bar{\epsilon} < 2.4 \times 10^{-1}$ cm^2 s^{-3} for the 100–120 m depth range. The Williams and Gibson (1974) $\bar{\epsilon}$ value, derived from a horizontal tow at 110 m, is well within the confidence interval shown in Table 1, even without correction for the fact that the mean velocity of the undercurrent was higher than that of Crawford (1982) by a factor of 2, which should increase $\bar{\epsilon}$ by a factor of about 8. Correcting for the difference in mean velocities brings the ratio of mean values to 2.3, which is remarkably good agreement considering that Crawford's mean value is uncertain within a factor of 2500 and that the Crawford (1982) measurements were above the core (150 m) and the Williams and Gibson (1974) measurements were at core depths.

It seems clear that the turbulence and mixing processes in the undercurrent have been vastly undersampled, and that estimates of mean values are quite uncertain. Vertical profiles of σ^2 in the undercurrent layers are needed, based on an appropriate number of *independent* samples of ϵ and χ. If the mean values are to represent space–time averages at some location, the samples in time must cover a full range of years, seasons of the year and times of the day, and the samples in space must cover several horizontal eddy lengths, where

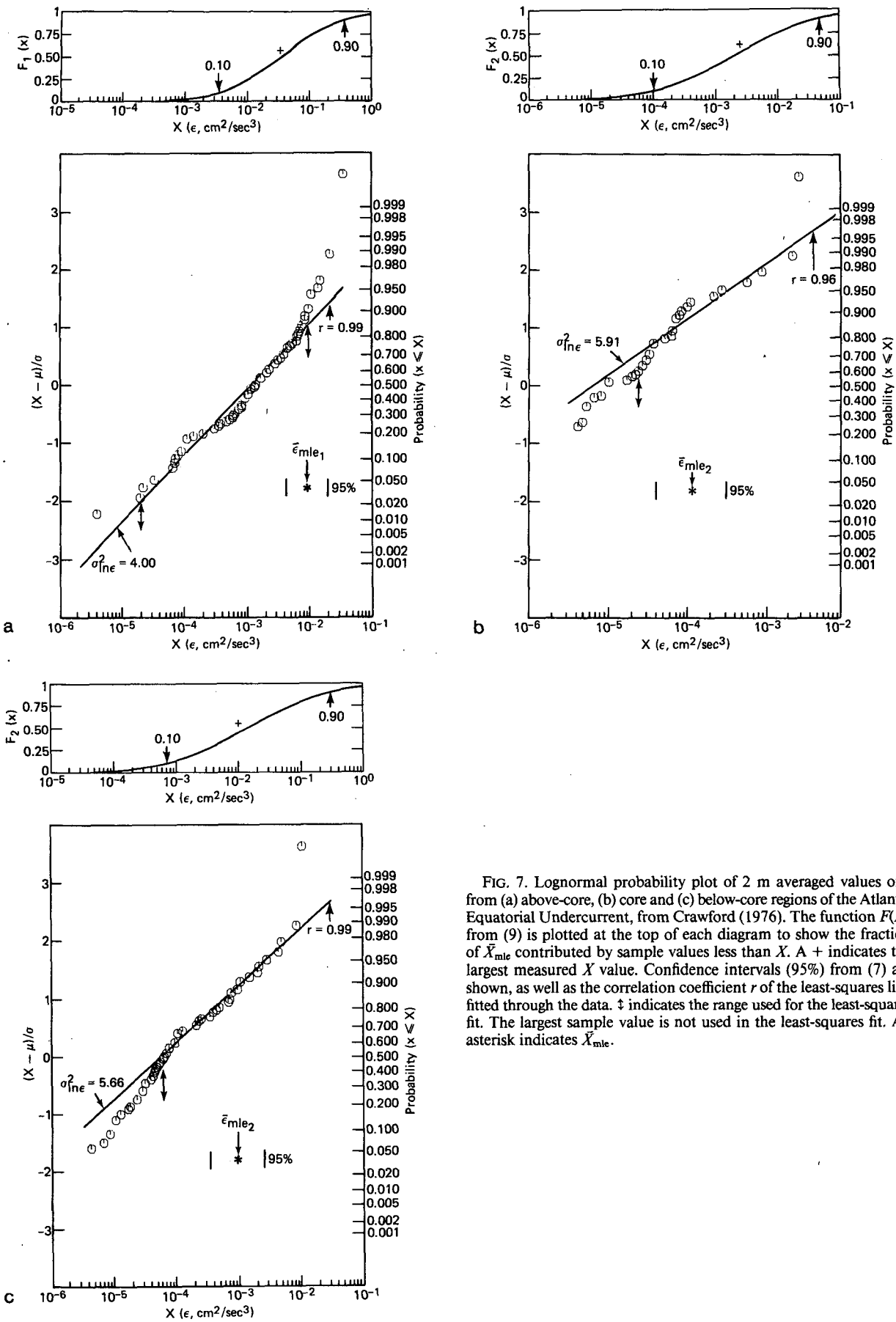

FIG. 7. Lognormal probability plot of 2 m averaged values of ϵ from (a) above-core, (b) core and (c) below-core regions of the Atlantic Equatorial Undercurrent, from Crawford (1976). The function $F(X)$ from (9) is plotted at the top of each diagram to show the fraction of $\bar{X}_{\text{mle}}$ contributed by sample values less than X. A + indicates the largest measured X value. Confidence intervals (95%) from (7) are shown, as well as the correlation coefficient r of the least-squares line fitted through the data. ‡ indicates the range used for the least-squares fit. The largest sample value is not used in the least-squares fit. An asterisk indicates $\bar{X}_{\text{mle}}$.

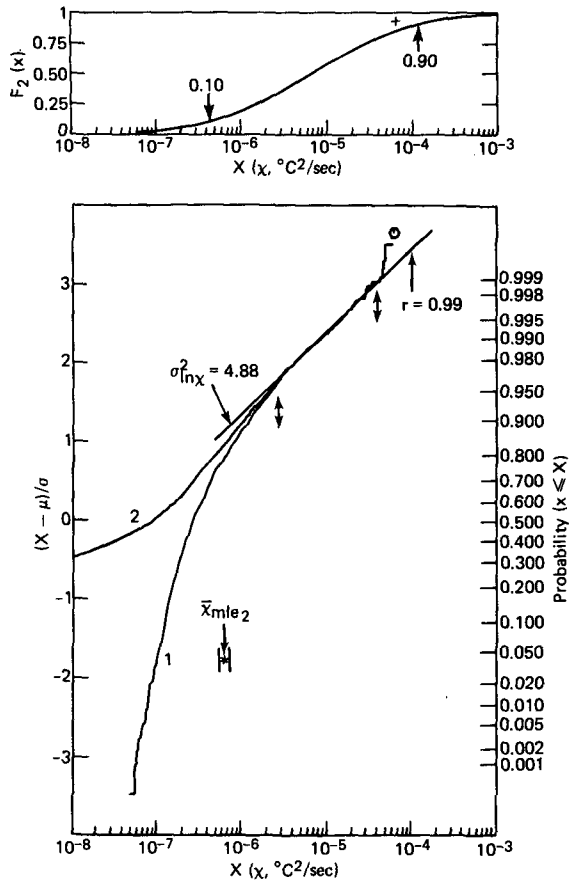

FIG. 8. Notation as in Fig. 7, for 1 m averaged contiguous samples of χ in the seasonal thermocline during MILE (medium winds), from Washburn and Gibson (1984). The CDF of the data, which includes noise, is indicated by 1 and the CDF generated by noise subtraction is indicated by 2. These curves should be compared to the correspondingly numbered simulated CDFs in Fig. 2.

eddy lengths at this latitude are about 500 km with convection times at core depths of about 4 days. Tendencies, often observed, for extreme ϵ and χ values to cluster in small regions of space (clouds) and small regions of time (storms) also complicate the process of obtaining a representative set of independent samples.

Figures 7a, b, c show lognormal probability plots of 2 m averaged ϵ values from the above-core, core and below-core regions of the Atlantic equatorial undercurrent from Crawford (1976). The sample values for each region, as defined by Crawford for each profile, are derived from the profiles of ϵ presented in Crawford (1976). The fraction of the record at the noise level or less was only 1% for the above-core region. Confidence intervals based on arithmetic means of $\mu_{\ln\epsilon}$ and $\sigma^2_{\ln\epsilon}$ are not seriously affected. The core layer measurements are in the noise for 23% of the total record. This forces the estimates to be made graphically. The simulation displayed in Fig. 1 also indicates that the CDF of the below-core data is significantly effected by noise. The confidence intervals displayed for the core and below-core regions in Fig. 7 are constructed using these graphical estimates.

The 95% confidence intervals for $\bar{\epsilon}$ based on $\bar{\epsilon}_{mle}$ estimates in the core and below-core zones overlap, which is contrary to the assertion by Crawford and Osborn (1980) that the core region is effectively nonturbulent and displays a minimum in dissipation compared to the shear zones above and below. The 95% confidence limits for the core and below-core regions are $3.8 \times 10^{-5} < \bar{\epsilon} < 3.2 \times 10^{-4}$ and $3.2 \times 10^{-4} < \bar{\epsilon} < 2.3 \times 10^{-3}$, respectively. The below-core region has an estimated $\bar{\epsilon}_{mle}$ of 8.6×10^{-4} cm^2 s^{-3} compared to 1.1×10^{-4} for the core. The least-squares fit for the core data indicates $\sigma^2_{\ln\epsilon}$ is 5.91 which implies a mean-to-mode ratio of 7080 for the core and indicates that a much larger sample is required for statistically significant statements about the relative levels of mixing in the layers of the Atlantic equatorial undercurrent.

According to the noise model discussed in section 5, the droop in the CDF in Fig. 7b below 6×10^{-5} cm^2 s^{-3} is probably due to noise effects. If the region above this droop represents the underlying CDF the model would predict that $\sigma^2_{\ln\epsilon}$ is probably much larger than

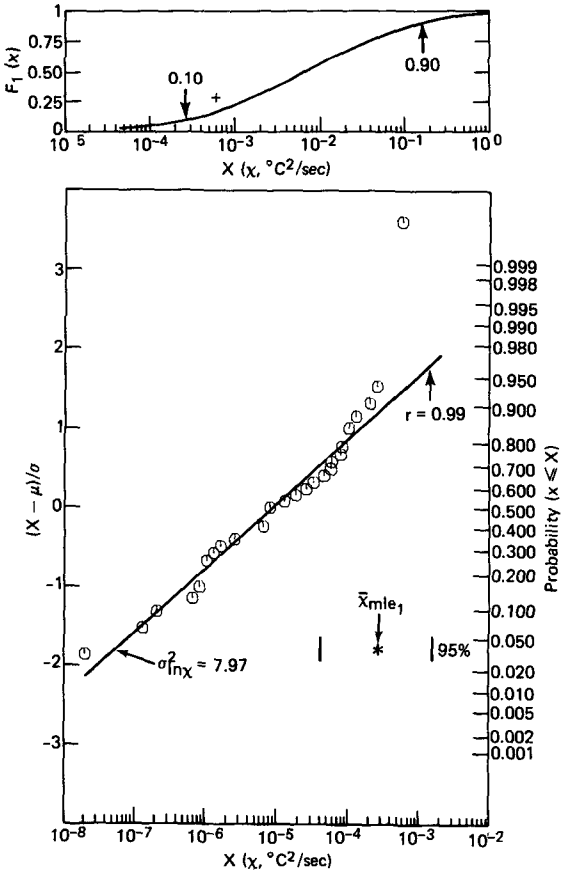

FIG. 9. As in Fig. 7 except for 0.5 m averaged contiguous values of χ in the seasonal thermocline during MILE (high winds), from Dillon (1982).

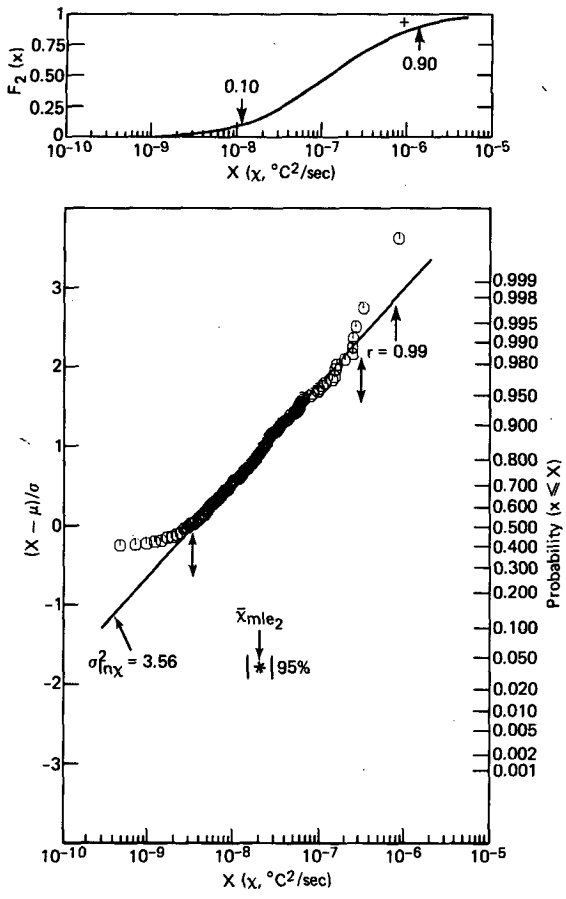

FIG. 10. As in Fig. 7 except for 10 m averaged χ values, corrected by noise subtraction, starting from the base of the seasonal thermocline, over the depth range 35 to 125 m, from Elliott and Oakey (1979). Compare with Fig. 3.

the previously cited (already enormous) value of 5.91 for the core region for this dataset.

b. Seasonal thermocline

Figure 8 displays the lognormal probability plot, mentioned in section 2, for χ measured in the horizontal direction with a towed body during the mixed layer experiment MILE, from Washburn and Gibson (1984). About 4 km of data, taken in the seasonal thermocline near ocean station PAPA over a two-hour period, are included in the plot, giving 3792 data samples. The temperature dissipation rate χ is averaged over approximately 1-meter segments and detected by a microconductivity probe. The use of this sensor to detect small-scale oceanic temperature fluctuations at high speed is described in Washburn and Gibson (1982).

As discussed in section 2, deviations from lognormality at low and high ends of the distribution can be attributed to noise, spatial resolution limitations and undersampling. Curve 1 demonstrates the effect of including noise and curve 2 shows the effect of noise subtraction. The least-squares fit to the resolved portion of the CDF gives $\sigma^2_{ln\chi} = 4.88$, $\mu_{ln\chi} = -16.74$ and estimated mode of 4×10^{-10} °C² s^{-1}. The estimated mean is $\bar{\chi} = 6.2 \times 10^{-7}$ °C² s^{-1}.

To illustrate the potential hazard of large undersampling errors in oceanic layers with large intermittency, these values are compared with χ values in the seasonal thermocline of 10^{-8}–10^{-9} °C² s^{-1} measured by Lange (1981) from a small number of drops during the same experiment. Lange's values are closer to the mode value of 4×10^{-10} °C² s^{-1} indicated by the lognormal fit to the towed-body data than to the indicated mean of 6.2×10^{-7} °C² s^{-1}. As shown in Fig. 5 of Gibson (1983), the individual χ profiles reported by Lange (1981) show a rapid decrease through the seasonal thermocline from a maximum at the base of the mixed layer, and are *qualitatively* different than the profile computed by averaging multiple dropsonde profiles of Dillon (1982), which shows that a *maximum* in $\bar{\chi}$ actually exists at the thermocline depth. A profile of $\sigma^2_{ln\chi}$ estimated from the Dillon (1982) data, in Fig. 7 of Gibson (1983), shows that the Lange maximum $\bar{\chi}$ occurs at a shallower depth where $\sigma^2_{ln\chi}$ has a minimum value of less than 1.0, whereas the value of $\sigma^2_{ln\chi}$ has a maximum (near 5) in the seasonal thermocline corresponding to minimal Lange χ values.

Figure 9 shows a lognormal probability plot of contiguous 50 cm averaged χ values taken with a dropsonde system during MILE, from Dillon (1982). These values are from a *single* profile through the ~30–40 m seasonal thermocline depth with wind speeds in excess of 15 m s^{-1}. Figure 9 indicates an extremely intermittent lognormal CDF with $\sigma^2_{ln\chi}$ of 6.5, highlighting the intermittency that can be present even within individual profiles.

Oakey kindly provided us with the individual 10 m averaged values of χ from all the drops and depths used in Elliott and Oakey (1979) for their fit of the Cox number to a lognormal. Figure 10 shows a lognormal probability plot of those 333 χ values. The depth range is from 35 to 125 m, starting just beneath the seasonal thermocline. A noise spectrum is estimated from the data near the termination of each drop. Noise subtraction is performed after a 10 m averaged spectrum is produced and any spectrum with a variance less than the noise level is set equal to zero, Elliott and Oakey (1979). About 30% of the 333 samples are in the noise. Based on the graphical estimates of $\mu_{ln\chi}$ of −19.48 and $\sigma^2_{ln\chi}$ of 3.56, $\bar{\chi}_{mle}$ is 2.06×10^{-8} °C² s^{-1} with an estimated 95% confidence interval of $1.6 \times 10^{-8} < \bar{\chi} < 2.7 \times 10^{-8}$. The arithmetic mean is 2.2×10^{-8} °C² s^{-1}, whether a value of zero, or a value equal to the smallest value shown in Fig. 10 (6×10^{-10}), is assigned to the 10 m samples below the noise level.

c. Main thermocline

The deep main thermocline microstructure measurements of Gregg (1977) from the northern mid-Pacific gyre are often interpreted to estimate the mean

vertical eddy diffusivity coefficient K_v ignoring any intermittency effects on the estimator of this quantity. Such estimates generally give K_v values one or two orders of magnitude smaller than canonical estimates of order 1 $cm^2\ s^{-1}$ from bulk property models such as in Munk (1966). For example, Jenkins (1980) cites an average value of $K_v = 0.01\ cm^2\ s^{-1}$ based on the Gregg (1977) data. Gregg and Briscoe (1979) state that, "Cox numbers high enough to support the $10^{-4}\ m^2\ s^{-1}$ diffusivity obtained in models such as Abyssal Recipes, Munk (1966), have not been found in midgyre oceanic regimes." The following reviews this dataset to see if such strong conclusions are warranted.

Cox numbers reported by Gregg (1977) are underestimates because the microstructure is treated as if it is completely anisotropic and vertically stratified. Gargett (1984) uniformly applies a thermistor frequency response correction factor of 2 and isotropic correction factor of 3 to the Cox numbers in the depth ranges of 0.2–0.6 km and 0.8–1.2 km, reported in Gregg (1977). This correction factor of 6 yields arithmetic mean Cox numbers of 42 and 354, respectively. The data from the deeper depth range, below the salinity minimum at 600 m, are appropriate for comparison to the canonical models which balance vertical diffusion with upwelling such as in Munk (1966). Applying Gargett's correction factor to Gregg's Cox numbers from this range results in an arithmetic mean Cox number of 276, and a vertical eddy diffusivity K_v of $0.4\ cm^2\ s^{-1}$. Gargett (1984) claims this value represents an upper bound on K_v because of possible violations of the Osborn–Cox model assumptions, such as the neglect of lateral advection of microstructure into the measuring area. However, the Gargett (1984) upper bound does not consider the possibility of underestimating the true mean through intermittency effects discussed above, or the large uncertainty associated with the use of the arithmetic mean of a small sample from a skewed distribution. An upper bound should be the sum of the maximum estimate of a parameter plus the maximum positive uncertainty of that estimate. The Gargett (1984) upper bound contains neither of these elements.

Using Gargett's factor of 6 to correct the Gregg (1977) data and using a lognormal probability plot indicates that the Cox number is an intermittent lognormal CDF with arithmetic estimates $\mu_{\ln C} = 4.67$ and $\sigma^2_{\ln C} = 2.25$. The maximum likelihood estimator assuming lognormality is $\bar{C}_{\text{mle}} = 329$ with corresponding $K_v = 0.46$. From (7), the 95% confidence interval based on this estimate is $82 < \bar{C}_{\text{mle}} < 1327$. Therefore, the correct upper bound indicated by the Gregg (1977) microstructure data (using the Gargett correction) is $K_v = 1.9\ cm^2\ s^{-1}$, not 0.4. As shown earlier, the confidence interval for the arithmetic mean is even larger, which increases the upper bound of K_v based on this estimator even further.

Gregg and Meagher (1980) retest the same brand of thermistor used in the midgyre expeditions and find that the data are *overcorrected* for thermistor response in Gregg (1977) using the Hacker correction (not *undercorrected* as assumed by Gargett, 1984). The Hacker correction is a 2-pole low-pass filter with a time constant of 35 ms. Gregg and Meagher (1980) report a 2-pole low-pass filter with a time constant of 21.7 ms as representative of these thermistors. This correction is used to reevaluate the Gregg (1977) spectra. By means of overlay and enlargement techniques, the original spectral values for the depth range of interest, 600–1200 m, are recovered from Fig. 9c, d in Gregg (1977) and are shown in Fig. 11. From these, the Hacker correction is removed and the new correction applied to give the improved spectral estimates shown in Fig. 12. All of the newly corrected spectra, including the most active data from MSR 20, now appear to have adequately resolved spectral peaks and show various degrees of diffusive rolloff. The spectra, in variance preserving form, are compared to the Batchelor spectrum. This comparison reveals that the variance computed from MSR7 (Tasaday 11), MSR10, and MSR20 require a 35% correction for unresolved variance. The other spectra are essentially fully resolved. Because the spectra are normalized by $(d\bar{T}/dz)^2$, integration of the spectra yield one-dimensional Cox numbers.

Figure 13 is a profile of the temperature gradient variance, from Gregg (1980). The 150-meter averaged

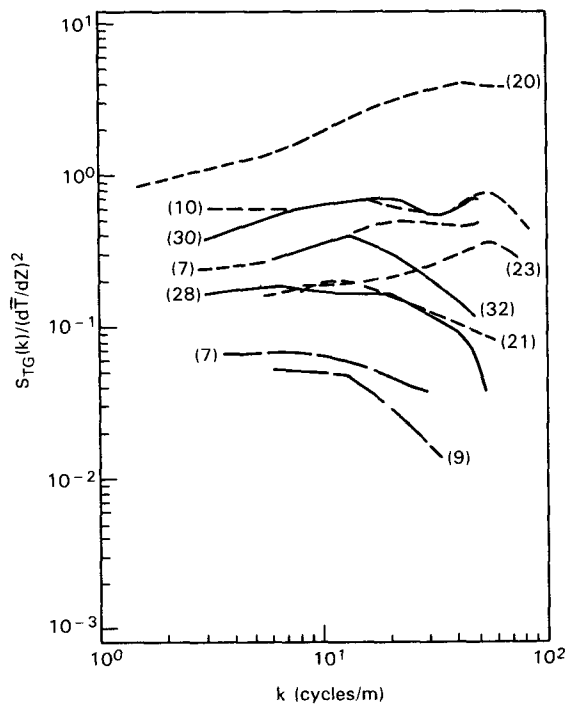

FIG. 11. Normalized temperature gradient spectra with original Hacker thermistor frequency response correction, from Gregg (1977). Curves long-dash, solid and short-dash correspond to drops from the *Aries* 9, *Tasaday* 1 and *Tasaday* 11 cruises, respectively. The drop or MSR number is shown in parenthesis for each curve.

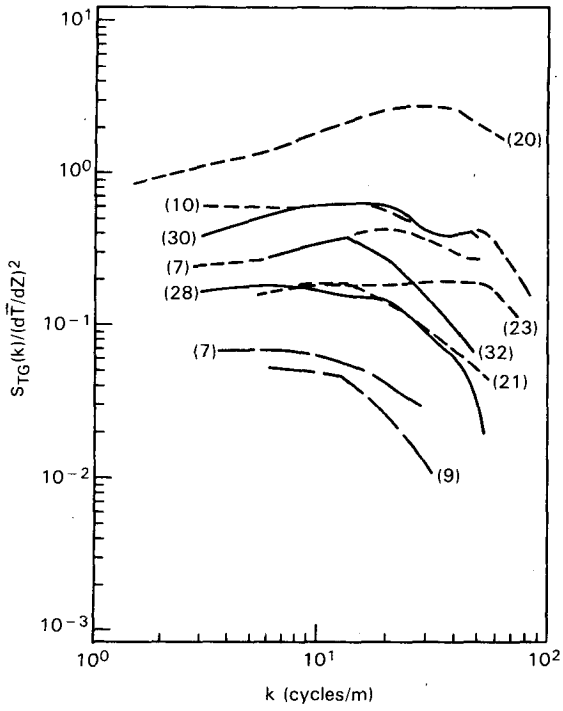

FIG. 12. Normalized temperature gradient spectra of Fig. 11 recorrected using the improved frequency response of Gregg and Meagher (1980).

Cox number $\bar{C}_{150\ m}$ for this profile reported by Gregg (1977) is 62. However, the dominant contribution to the average is from active segments with a summed length less than 10 meters. In these segments the Cox number is several hundred and the scales dominating the temperature gradient variance within these segments should be isotropic, so that the correct value of $\bar{C}_{150\ m}$ should have been 186. Based on such profiles, all $\bar{C}_{150\ m}$ larger than 30 are corrected by a factor of 3 to account for isotropy. However, the smallest $\bar{C}_{150\ m}$ values, some of which are less than 2, are not corrected for isotropy because the profiles are basically inactive and the "microstructure" is completely vertically stratified. Corrections for isotropy for $\bar{C}_{150\ m}$ values in the range 2–30 are somewhat arbitrary, but have little effect on the resulting probability plots and their indicated distribution functions.

Figure 14 displays both normal and lognormal probability plots for the $\bar{C}_{150\ m}$ values of Gregg (1977), corrected for isotropy and the improved frequency response of Gregg and Meagher (1980) as described above. The fit to normal is exceedingly poor (curved line), and the fit to a very intermittent lognormal CDF (straight line) is quite good.

Assuming lognormality, the graphical method for the corrected values yields $\bar{C}_{mle} = 181$ with $\mu_{\ln C} = 2.6$ and $\sigma^2_{\ln C} = 5.2$. The arithmetic method produces $\bar{C}_{mle} = 179$ with $\mu_{\ln C} = 2.98$ and $\sigma^2_{\ln C} = 4.41$. The corresponding value of K_v is 0.25 cm^2 s^{-1}. The 95% confidence interval for $\bar{C}$, based on the values $\mu_{\ln C} = 2.98$ and $\sigma^2_{\ln C} = 4.41$, is $16 < \bar{C} < 2003$. The corresponding interval for the vertical eddy diffusivity is $0.02 < K_v < 2.8$ cm^2 s^{-1}. Therefore, considering the intermittent lognormality of the microstructure, no statistically significant discrepancy is found between the (microstructure) K_v values indicated by the Gregg (1977) data and the canonical estimates of K_v from bulk property models such as Munk (1966).

In order to make meaningful comparisons between K_v estimates derived from deep ocean microstructure measurements and canonical values derived from bulk properties, much larger microstructure datasets will be required. If the indicated σ^2 of about 5 for $\bar{C}_{150\ m}$ is correct, as indicated by the Gregg (1977) data, about 240 independent samples must be collected to give a factor of 2 uncertainty at the 95% level to estimate $\bar{C}$ in the main thermocline by this method. Over 1000 samples would be necessary for a 20% uncertainty.

5. Discussion of results

Why are oceanic dissipations rates lognormal, and why are they so intermittent? Intermittent lognormality is a characteristic of nonlinear random variables, such as high Reynolds number turbulence dissipation, droplet or particle size, rare metal concentration in the

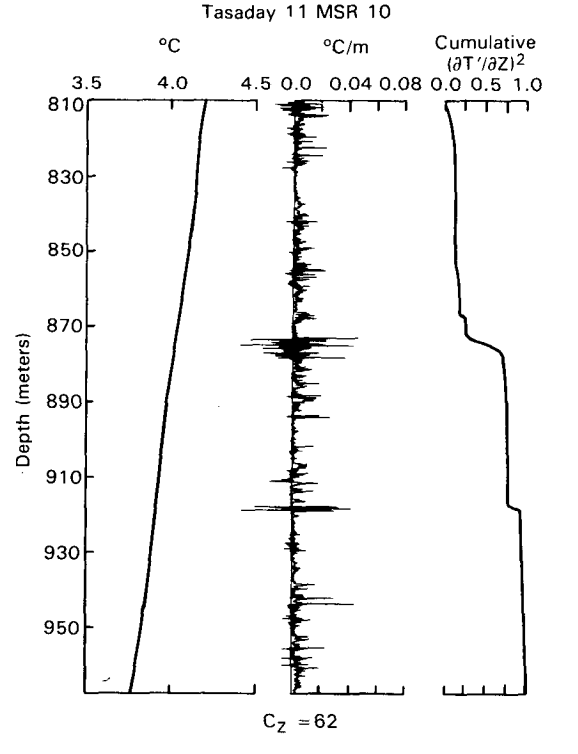

FIG. 13. Profiles of temperature, temperature gradient and cumulative temperature gradient variance from Gregg (1980). The mean Cox number is 62 with most of the mean value contributed by regions where C is several hundred and presumably isotropic.

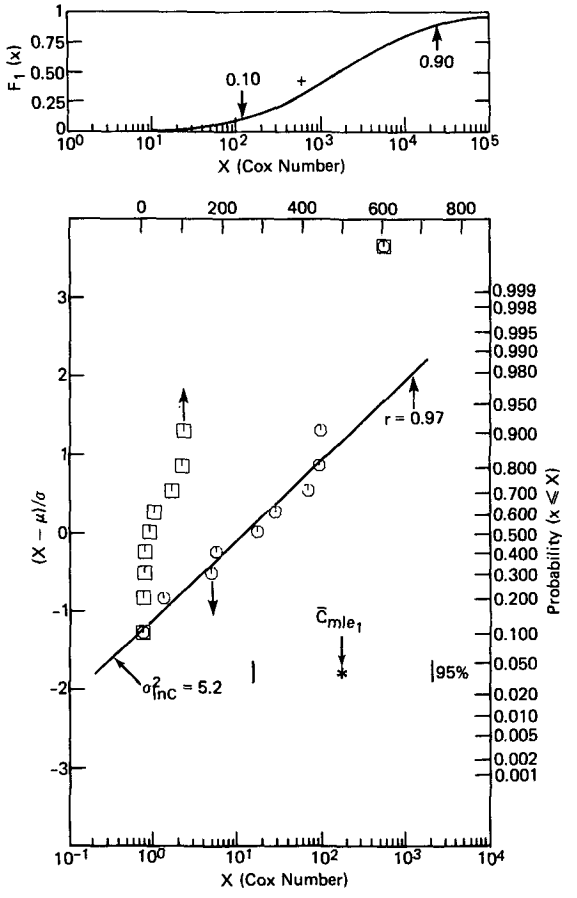

FIG. 14. Lognormal (O) and normal (Δ) probability plots of $\bar{C}_{150\ m}$ values corrected for isotropy and frequency response, for the depth range 600–1200 m, from Gregg (1977). The data are clearly not normal, but strongly indicate a lognormal (straight line) CDF. The notation is the same as Fig. 7.

earth crust, or personal income, which are at the end of a long chain, or cascade, of independent, multiplicative events. Lognormality of ϵ in high Reynolds number turbulence is proposed by Kolmogoroff (1962) as a refinement to the first and second universal similarity hypotheses of Kolmogoroff (1941). The "third hypothesis" of Kolmogoroff (1962) may be written as

$$\sigma^2_{\ln\epsilon} = \mu \ln[L_{\text{energy}}/L_{\text{dissipation}}] \qquad (10)$$

where μ is a universal constant. Hot wire measurements of ϵ in the atmospheric boundary layer over the ocean by Gibson et al. (1970) show good agreement with the Kolmogoroff lognormal hypothesis. Maximum values of $\sigma^2_{\ln\epsilon}$ of about 4.0 were detected for the highest winds at a maximum height of 30 meters above the sea. The constant μ was found to be $\sim$0.5.

Gurvich and Yaglom (1967) show that lognormality of ϵ follows from the central limit theorem and a cascade model of turbulence covering a wide range of independent eddy length scales from L_{energy} to $L_{\text{dissipation}}$. Gibson (1981) extends the Gurvich and Yaglom cascade model to explain the observed lognormality of $X \equiv \epsilon$ and χ in the ocean. According to the model, $\sigma^2_{\ln X}$ in a stratified layer should increase logarithmically with the range of horizontal eddy scales as

$$\sigma^2_{\ln X} = \mu' \ln[L_{\text{energy}}/L_{\text{buoyancy}}] \qquad (11)$$

where μ' is a constant $\approx \mu$, L_{energy} is the largest horizontal eddy scale, usually limited by Coriolis forces, and L_{buoyancy} is the largest vertical eddy scale, usually limited by buoyancy forces. Horizontal eddies may cover meters to megameters in the ocean and thus possibly account for the wide range of $\sigma^2_{\ln X}$ values, using the above expression. However, at this time none of the terms on the right-hand side of the expression are known well enough in any layer of the ocean to provide better than crude comparisons to measured values on the left-hand side. The observation that intermittency factors are maximum in layers with maximum stratification is consistent with the cascade model of intermittency because the ratio $L_{\text{energy}}/L_{\text{buoyancy}}$ should be maximum in such layers. The observation that intermittency factors are small in the surface mixing layer and in shear layers is also consistent, because the energy scale of the horizontal eddies in such layers is relatively small, comparable to the layer thicknesses, and the buoyancy scales are relatively large.

In section 4 several microstructure datasets from the Atlantic and Pacific equatorial undercurrents, the seasonal thermocline and the main thermocline were reviewed to test the validity and consequences of the hypothesis of lognormality in the ocean. Each of these layers is strongly stratified relative to the layers above and below and, perhaps as a consequence of the stratification, the turbulence and mixing parameters $X \equiv \epsilon$, χ and C are extremely intermittent with $\sigma^2_{\ln X}$ in the range 3–7 and distribution functions that are indistinguishable from lognormal. Because the datasets are small, the confidence intervals for $E(X)$ are generally very wide, indicating severe undersampling. Several anomalous results and discrepancies in estimates of mean values between datasets are resolved when this undersampling due to intermittency is taken into account. Except for the Washburn and Gibson (1984) seasonal thermocline data and the below-core data from Crawford (1976), the function $F(X)$ also indicates the remaining reviewed datasets are undersampled.

The most extreme intermittency was found in the equatorial undercurrent high-velocity core layers. Maximum values of $\sigma^2_{\ln\chi}$ and $\sigma^2_{\ln\epsilon}$ possibly result from the combined effects of the strong stratification of the layer, the high velocities of the undercurrent and the large horizontal eddy scales at this latitude resulting from large velocities and minimum constraining Coriolis forces. Large apparent discrepancies between undercurrent mean dissipation rates indicated by towed-body and dropsonde measurements have remained unresolved for over a decade and have been attributed by Gibson (1981, 1983) to intermittency effects. Anal-

ysis of the intermittency of equatorial microstructure measurements in section 4 is consistent with this interpretation. Inferred minima in mean dissipation rates at undercurrent core depths may be artifacts of undersampling errors due to intermittency because, from the lognormal confidence intervals derived in section 3, these minima lack statistical significance.

The largest available datasets have been collected in the seasonal thermocline. Apparent minima in the vertical profiles of mean temperature dissipation rates $\bar{\chi}$ at the seasonal thermocline depth result from maximum undersampling errors in this layer of maximum intermittency. Adequately sampled profiles of $\bar{\chi}$ actually show *maximum* values at this depth, as shown in section 4 and in Gibson (1983).

It is commonly accepted that a discrepancy exists between the vertical eddy diffusivity K_v indicated by the main thermocline microstructure measurements of Gregg (1977), setting $K_v = DC$, and canonical estimates of K_v from bulk properties. Gregg and Briscoe (1979) and Jenkins (1980) point out this discrepancy and estimate that K_v from the microstructure measurements is one or two orders of magnitude less than values of $K_v = 1.0$ cm^2 s^{-1} inferred from bulk property models such as Munk (1966). When the extreme intermittency and lognormal probability distribution indicated by the Gregg (1977) data are taken into account, the discrepancy is statistically insignificant because the confidence interval for K_v is very wide, due to undersampling, and includes both estimates.

6. Conclusions

Presently available microstructure datasets in stratified oceanic layers indicate that the probability distribution functions describing turbulence and mixing parameters ϵ, χ, and the Cox number are indistinguishable from highly intermittent lognormal CDFs. Monte Carlo simulations show that apparent deviations from lognormality of the empirical oceanic CDFs are explained by a simple model based on noise and sample size effects.

For lognormal random variables the arithmetic mean $\bar{X}_{am}$ is shown (in appendix B) to be an extremely inefficient estimator of the expected value $E(X) = \bar{X}$ compared to the maximum likelihood estimator $\bar{X}_{mle}$ for intermittency factors $\sigma^2_{\ln X} > 3.0$, and can greatly underestimate $E(X)$ if small datasets are used. Confidence intervals are derived for $\bar{X}_{mle}$ which indicate that 2600 or 10 000 independent samples are required for statistically significant estimates of expected values for $\sigma^2_{\ln X}$ values of 3 or 7, respectively.

From these confidence intervals, minima in turbulent mixing rates and vertical eddy diffusivities at the high-velocity core depths of the Atlantic equatorial undercurrent inferred by Crawford and Osborn (1980) appear to be artifacts of the sampling technique employed, which undersamples the turbulence and mixing processes in such extremely intermittent layers.

The supposed discrepancy between small values for the deep main thermocline eddy diffusivity, estimated from microstructure data of Gregg (1977), and the canonical values of $K_v \approx 1$ cm^2 s^{-1}, estimated from bulk flow models such as Munk (1966), is rejected under the hypothesis that the data are lognormally distributed. After correction for isotropy and sensor frequency response, the Gregg (1977) Cox number values are shown to be highly non-Gaussian and in good agreement with an intermittent lognormal CDF. The 95% level confidence interval for $\bar{C}$ corresponds to a confidence interval for the vertical eddy diffusivity of $0.02 < K_v < 2.8$ cm^2 s^{-1}.

Acknowledgments. We would like to thank our colleagues for many helpful discussions. Neal Oakey was particularly kind to provide the original data used in Elliott and Oakey (1979). Support for this research was provided by the Office of Naval Research Contract N00014-85-C-0104 and by a grant from the University of California at San Diego Committee for Academic Research. We are grateful for a number of helpful comments provided by Mel Briscoe and other reviewers of the original version of this paper.

APPENDIX A

Properties of Lognormal Random Variables

If a random variable X is lognormally distributed, then $\ln X$ is normally distributed with expected value μ and variance σ^2. The probability density function (pdf) of X is

$$f(x) = \frac{1}{(x\sigma\sqrt{2\pi})} \exp\left[\frac{-(\ln x - \mu)^2}{2\sigma^2}\right]. \quad \text{(A1)}$$

The ith moment of X is

$$E(X^i) = \exp\left(i\mu + \frac{i^2\sigma^2}{2}\right). \quad \text{(A2)}$$

The expected value of X is

$$E(X) = \exp\left(\mu + \frac{\sigma^2}{2}\right). \quad \text{(A3)}$$

The mode of X, or the most probable value of X, is

$$\text{mode}(X) = \exp(\mu - \sigma^2). \quad \text{(A4)}$$

The median of X is

$$\text{median}(X) = \exp(\mu). \quad \text{(A5)}$$

The variance of X is

$$\text{var}(X) = \exp(2\mu + \sigma^2)[\exp(\sigma^2) - 1]. \quad \text{(A6)}$$

Unlike the normal distribution, which has a constant mean-to-mode ratio of unity, it follows from (A3) and (A4) that the lognormal distribution has a variable mean-to-mode ratio R,

$$R = [\text{mean/mode}]_{\text{LNrv}} = \exp(3\sigma^2/2) \qquad \text{(A7)}$$

that increases exponentially with the intermittency factor σ^2. This relation is shown in Fig. A1. By its definition, in (A4), the most probable value of a single datum (or, approximately, the average of a small sample set) is the mode, which severely underestimates the mean if σ^2 is large, as shown in Fig. A1. Equations (A3), (A4) and (A5) show that $E(X) >$ median $>$ mode for the lognormal distribution, in contrast to the relation

$$E(X) = \text{median} = \text{mode}$$

when the distribution is normal.

Figure A2 displays the dramatic effect of $\sigma^2_{\ln X}$ on the shape of the lognormal distribution. In Fig. A2, lognormal pdfs normalized by their modal values are shown for several values of $\sigma^2_{\ln X}$. For $\sigma^2_{\ln X} = 1$, the mean value is easily shown on the plot. However, for $\sigma^2_{\ln X} = 5.0$, the mean value would be several meters off the page to the right. Because the shape of the pdf and the mean-to-mode ratio depend only on $\sigma^2_{\ln X}$, $\sigma^2_{\ln X}$ determines the numbers of samples necessary to achieve a given accuracy in estimating any statistical parameter of the distribution, and is therefore the parameter which should motivate the sampling strategy. Increased intermittency in X is reflected in larger values of $\sigma^2_{\ln X}$. Consequently, $\sigma^2_{\ln X}$ measures the intermittency of X and is referred to in this paper as the intermittency factor of the LNrv.

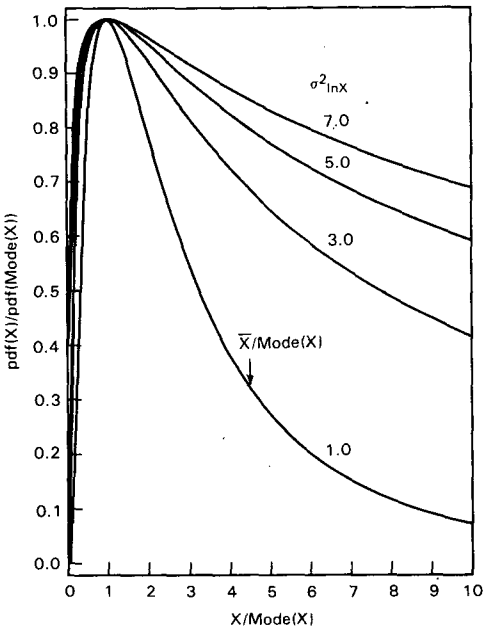

FIG. A2. Lognormal pdfs normalized by the peak value of the pdf that occurs at the mode, for various intermittency factors, plotted versus the random variable normalized by the modal value.

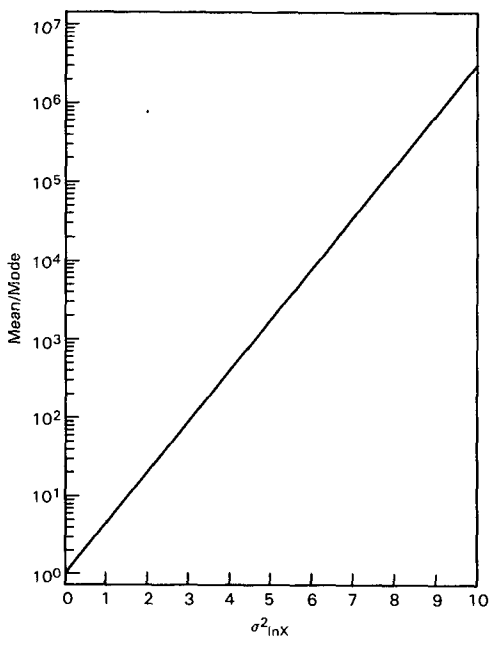

FIG. A1. Mean-to-mode ratio versus intermittency factor for lognormal random variables, from (7). This ratio represents the *probable* correction factor required for small microstructure datasets used to estimate mean values neglecting the intermittent lognormality of oceanic microstructure.

Data may be compared to a normal probability distribution function by plotting the fraction of the data less than or equal to various values of x on a "normal probability plot." The vertical axis is stretched so that data from a normal distribution fall about a straight line. The ordinate is the "standardized normal random variable" $Z \equiv (X - \mu)/\sigma$; that is, the value Z of a Gaussian with zero mean and unity variance with empirical probability $P(Z \leq x)$ equal to the measured fraction of data samples less than or equal to x. The probability associated with the largest observed sample value, 1.0 for the less than or equal sorting procedure, is arbitrarily set at 0.9999 in order to allow that sample value to appear on the probability plot. Lognormal probability plots replace the linear abscissa with a logarithmic axis. Such plots enable estimation of $\mu_{\ln X}$ and $\sigma^2_{\ln X}$. For the fitted line, the abscissa value, where $Z = 0$, yields an estimate of $\mu_{\ln X}$, and the square of the inverse of the slope provides an estimate of $\sigma^2_{\ln X}$. This method of estimating $\mu_{\ln X}$ and $\sigma^2_{\ln X}$ is referred to as the "graphical method" in this paper. Each of the oceanic datasets reviewed in this paper is compared to lognormality on a lognormal probability plot. The less than or equal sorting procedure forces the largest sample value to be excluded from the graphical procedure. For sample sizes of 100, the cumulative distribution functions of $\bar{X}_{\text{mle}}$ estimates produced by the arithmetic and graphical procedure are shown in Fig. 4b to be virtually indistinguishable.

APPENDIX B

Estimation of the Expected Value of a Lognormal Distribution

Given a pdf for a random variable X, several criteria may be used to select the best estimator of a statistical property of X, such as the expected value $E(X)$, from the possible estimators available. As a minimum set of criteria, the various estimators should be evaluated as to their consistency, bias and relative efficiency. If possible, confidence intervals should be available to express the degree of uncertainty in the estimate.

A consistent estimator is one that converges in probability to the true value as the sample size $n \to \infty$. An estimator whose expected value equals the true value for any sample size is unbiased. An estimator whose expected value equals the true value as $n \to \infty$ is asymptotically unbiased.

The efficiency of an unbiased estimator $\hat{\alpha}$ relative to an unbiased estimator $\hat{\beta}$ is a measure of the relative number of samples required to achieve the same degree of uncertainty in $\hat{\alpha}$ as in $\hat{\beta}$. By definition, the relative efficiency of $\hat{\alpha}$ compared to $\hat{\beta}$ is

$$\mathrm{re}(\hat{\alpha}|\hat{\beta}) = \frac{D^2(\hat{\beta})}{D^2(\hat{\alpha})} \tag{B1}$$

where D^2 is used to indicate the variance of an estimator.

According to Freund (1971), if one or both of the estimators in question is biased the mean-square error of the biased estimator should be used in (B1) instead of the variance to evaluate the relative efficiency. The mean-square error of an estimator is given by

$$\mathrm{mse}(\hat{\alpha}) = E[(\hat{\alpha} - \alpha)^2] \tag{B2}$$

where α is the true value. Equation (B2) may be rewritten by substituting the identically zero expression $E(\hat{\alpha}) - E(\hat{\alpha})$ inside the squared term and rearranging terms to yield

$$\mathrm{mse}(\hat{\alpha}) = D^2(\hat{\alpha}) + [E(\hat{\alpha}) - \alpha]^2. \tag{B3}$$

The last term is the square of the bias of $\hat{\alpha}$. Note that for an asymptotically unbiased estimator the mean-square error and the variance converge as $n \to \infty$.

According to Cramer (1946), the method of maximum likelihood produces, under general conditions, a consistent estimator that is at least asymptotically unbiased and possesses minimal variance. The basic method is to form the likelihood function L for a sample of n independent values from a population of the continuous type,

$$L(x_1, \ldots, x_n; \theta) = f(x_1, \ldots, x_n; \theta) = \prod_{i=1}^{n} f(x_i; \theta) \tag{B4}$$

where $f(x_1, \ldots, x_n; \theta)$ is the probability of obtaining the particular sample $(x_1, \ldots, x_n)$ given that θ is a parameter of the population. Given the sample values, the likelihood function is only a function of θ, $L = L(\theta)$. The value of θ for which the likelihood function is maximum, thereby maximizing the probability of obtaining such a sample, is the "maximum likelihood estimator" θ_{mle} which is found where

$$\frac{\partial \ln L}{\partial \theta} = 0. \tag{B5}$$

The value of θ_{mle} depends on the sample $x_1, \ldots, x_n$. In the case of Nrvs, it may easily be shown that the maximum likelihood estimators of the true mean and variance are the arithmetic sample mean and arithmetic sample variance, respectively.

In the lognormal case, the maximum likelihood estimator of $E(X)$ is

$$\bar{X}'_{\mathrm{mle}} = \exp\left(m + \frac{s'^2}{2}\right) \tag{B6}$$

where m is the arithmetic sample mean

$$m = \frac{1}{n} \sum_{j=1}^{n} \ln X \tag{B7}$$

and s'^2 is the arithmetic sample variance

$$s'^2 = \frac{1}{n} \sum_{j=1}^{n} (\ln X - m)^2 \tag{B8}$$

from Kendall and Stuart (1967). The minimum variance unbiased estimator of $\sigma^2_{\ln X}$ is $s^2 = (n/n-1)s'^2$. In this paper $\bar{X}_{\mathrm{mle}}$ is used instead of $\bar{X}'_{\mathrm{mle}}$, where $\bar{X}_{mle}$ is defined by replacing s'^2 by s^2 in (B6); that is,

$$\bar{X}_{\mathrm{mle}} \equiv \exp\left(m + \frac{s^2}{2}\right). \tag{B9}$$

Estimation of $\mu_{\ln X}$ and $\sigma^2_{\ln X}$ by m and s^2, respectively, is referred to as the arithmetic method in this paper.

The arithmetic mean, median and mode are all excellent estimators of the expected value for Nrvs. Because all three are consistent and unbiased, the arithmetic mean is chosen as the best estimator on the basis of relative efficiency. Microstructure parameters are not Nrvs. Over the range where neither noise, spatial response or lack of samples contaminates the sample pdf, the data are lognormal.

The arithmetic mean of LNrvs, $\bar{X}_{\mathrm{am}}$, is unbiased and converges to the true value if the sample size is large enough. The variance of $\bar{X}_{\mathrm{am}}$ is

$$D^2(\bar{X}_{\mathrm{am}}) = \frac{\exp(2\mu + \sigma^2)[\exp(\sigma^2) - 1]}{n} = [\exp(\sigma^2) - 1]\frac{E^2(X)}{n} \tag{B10}$$

and the variance of $\bar{X}_{\mathrm{mle}}$ is

$$D^2(\bar{X}_{\text{mle}}) = \exp\left(2\mu + \frac{\sigma^2}{n}\right)\left[\exp\left(\frac{\sigma^2}{n}\right)\left(1 - \frac{2\sigma^2}{n-1}\right)^{-[(n-1)/2]} - \left(1 - \frac{\sigma^2}{n-1}\right)^{-(n-1)}\right] \quad \text{(B11)}$$

for $[1 - 2\sigma^2/(n-1)] > 0$, from Sichel (1951).

The expected value of $\bar{X}_{\text{mle}}$ is

$$E(\bar{X}_{\text{mle}}) = \exp\left(\frac{-(n-1)}{2n}\sigma^2\right)\left[\left(1 - \frac{\sigma^2}{n-1}\right)^{-[(n-1)/2]}\right]E(X) \quad \text{(B12)}$$

for $[1 - \sigma^2/(n-1)] > 0$. $\bar{X}_{\text{mle}}$ is positively biased but asymptotically unbiased.

The mean-square error of $\bar{X}_{\text{mle}}$ may be derived by directly evaluating (B2) or by combining (B3), (B11) and (B12). The mean square error of $\bar{X}_{\text{mle}}$ is

$$\text{mse}(\bar{X}_{\text{mle}}) = E^2(X)\left[1 + \exp\left(\frac{2-n}{n}\sigma^2\right)\left(1 - \frac{2\sigma^2}{n-1}\right)^{-[(n-1)/2]} - 2\exp\left(\frac{1-n}{2n}\sigma^2\right)\left(1 - \frac{\sigma^2}{n-1}\right)^{-[(n-1)/2]}\right] \quad \text{(B13)}$$

for $[1 - 2\sigma^2/(n-1)] > 0$. Therefore, from (B1), the relative efficiency $\text{re}(\bar{X}_{\text{am}}|\bar{X}_{\text{mle}})$ is given by the ratio of (B13) to (B10), and is shown by the solid curves in Fig. B1 for several sample sizes as a function of σ^2. Note that $E^2(X)$ divides out of the relative efficiency. Figure B1 demonstrates that $\bar{X}_{\text{am}}$ is extremely inefficient for the range of $\sigma^2_{\ln X}$ of about 3–7 commonly observed in oceanic microstructure measurements.

The small effect of the bias of $\bar{X}_{\text{mle}}$ on the relative efficiency is demonstrated by the comparison of the dotted curves in Fig. B1 with the solid curves. The dotted curves are generated by the ratio of $D^2(\bar{X}_{\text{mle}})/D^2(\bar{X}_{\text{am}})$.

Finney (1941) derives the minimum variance unbiased estimator, $\bar{X}_{\text{mvue}}$, which is a slowly converging series

$$\bar{X}_{\text{mvue}} = \exp(m)\left[1 + \frac{s^2}{2} + \frac{n-1}{2^2 2!}\frac{s^4}{(n+1)} + \frac{(n-1)^2 s^6}{2^3 3!(n+1)(n+3)} + \cdots\right] \quad \text{(B14)}$$

where m is defined by (B7) and s^2 is the minimum variance unbiased estimator of $\sigma^2_{\ln X}$.

According to Aitchison and Brown (1957), "Theory provides no means of obtaining exact confidence intervals for" $E(X)$ and $D^2(X)$. They suggest the assumption that estimators of $E(X)$ are asymptotically normal with mean $E(X)$ and variance $D^2(\text{estimator})$,

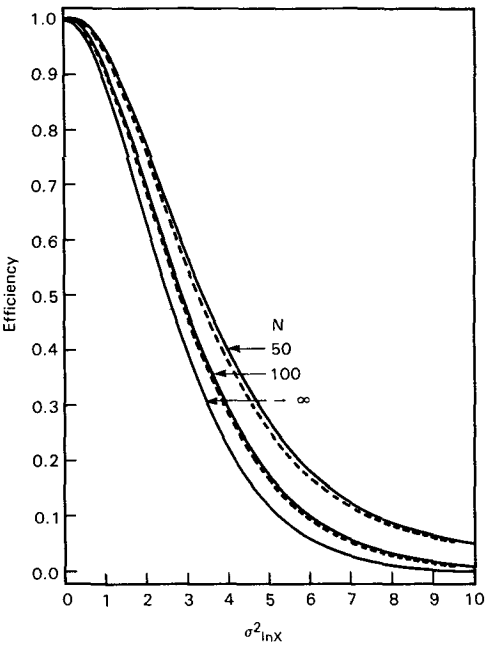

FIG. B1. Relative efficiency of the arithmetic mean vs the maximum likelihood estimator of the mean for LNrvs: (solid) re = mse $[\bar{X}_{\text{mle}}]/D^2[\bar{X}_{\text{am}}]$ from the ratio of (B13) to (B10); (dotted) re = $D[\bar{X}_{\text{mle}}]/D^2[\bar{X}_{\text{am}}]$ from the ratio of (B11) to (B10). N is the sample size.

respectively. The asymptotic variance of $\bar{X}_{\text{am}}$ is given by (B10) and for both $\bar{X}_{\text{mle}}$ and $\bar{X}_{\text{mvue}}$ the asymptotic variance may be expressed as $\exp(2\mu + \sigma^2)(\sigma^2 + \sigma^4/2)/n$, from Kendall and Stuart (1967), so that confidence intervals may be constructed as suggested by Aitchison and Brown with the familiar form

$$\text{estimator} - D(\text{estimator})z_{\alpha/2} < E(X) < \text{estimator} + D(\text{estimator})z_{\alpha/2} \quad \text{(B15)}$$

with a $(1 - \alpha)$ confidence coefficient. The large sample confidence interval based on $\bar{X}_{\text{am}}$ may be obtained in the same manner assuming that $\bar{X}_{\text{am}}$ is normally distributed for a large sample size. Small-sample confidence intervals for $\bar{X}_{\text{mle}}$ are derived in section 3 and are not presently available for either $\bar{X}_{\text{mvue}}$ or $\bar{X}_{\text{am}}$ at this time.

Based on relative efficiency (which includes bias effects), its convergence to the true value, and the availability of confidence intervals even for small sample sizes, $\bar{X}_{\text{mle}}$ is selected to estimate $E(X)$ for the intermittent oceanic dissipation parameters considered in the present paper.

REFERENCES

Aitchison, J., and J. A. C. Brown, 1957: *The Lognormal Distribution.* Cambridge University Press, 176 pp.

Belyaev, V. S., A. N. Gezentsvey, A. S. Monin, R. V. Ozmidov and V. T. Paka, 1975a: Spectral characteristics of small-scale fluc-

tuations of hydrophysical fields in the upper layer of the ocean. *J. Phys. Oceanogr.*, **5**, 492–498.
——, M. M. Lubimtzev and R. V. Ozmidov, 1975b: The rate of dissipation of turbulent energy in the upper layer of the ocean. *J. Phys. Oceanogr.*, **5**, 499–505.
Cramer, H., 1946: *Mathematical Methods of Statistics.* Princeton University Press, 575 pp.
Crawford, W. R., 1976: Turbulent energy dissipation in the Atlantic equatorial undercurrent. Ph.D. dissertation, The University of British Columbia, Canada, 149 pp.
——, 1982: Pacific equatorial turbulence. *J. Phys. Oceanogr.*, **12**, 1137–1149.
——, and T. R. Osborn, 1980: Microstructure measurements in the Atlantic equatorial undercurrent during GATE. *Deep-Sea Res.*, **26**, (GATE Suppl. II), 285–308.
——, and ——, 1981: Turbulence in the equatorial Pacific ocean. *Pac. Mar. Sci. Rep. 81-1*, Institute of Ocean Sciences, Sidney, B.C.
Dillon, T. M., 1982: Vertical overturns: A comparison of Thorpe and Ozmidov length scales. *J. Geophys. Res.*, **87**, 9601–9613.
Elliott, J. A., and N. S. Oakey, 1979: Average microstructure levels and vertical diffusion for Phase III, GATE. *Deep-Sea Res.*, **26** (GATE Suppl. I), 279–294.
——, and ——, 1980: The variability of temperature gradient microstructure observed in the Denmark Strait. *J. Geophys. Res.*, **85**, 1933–1944.
Finney, D. J., 1941: On the distribution of a variate whose logarithm is normally distributed. *J. R. Statist. Soc. B.*, **7**, 155–161.
Freund, J. E., 1971: *Mathematical Statistics.* Prentice-Hall, Inc., 463 pp.
Gargett, A. E., 1984: Vertical eddy diffusivity in the ocean interior. *J. Mar. Res.*, **42**, 359–393.
Gibson, C. H., 1980: Fossil temperature, salinity, and vorticity turbulence in the ocean. *Marine Turbulence*, J. C. J. Nihoul, Ed., Elsevier, 221–257.
——, 1981: Buoyancy effects in turbulent mixing; sampling turbulence in the stratified ocean. *Am. Inst. Aeronaut. Astronaut. J.*, **19**, 1394–1400.
——, 1982a: Alternative interpretations for microstructure patches in the thermocline. *J. Phys. Oceanogr.*, **12**, 374–383.
——, 1982b: On the sampling of vertical temperature gradient spectra. *J. Geophys. Res.*, **87**, 8031–8038.
——, 1982c: Fossil turbulence in the Denmark Strait. *J. Geophys. Res.*, **87**, 8039–8046.
——, 1983: Turbulence in the core of the equatorial undercurrent. *Hydrodynamics of the Equatorial Ocean, Proc. of the 14th Int. Liege Colloq. on Ocean Hydrodynamics*, Liege, J. C. Nihoul, Ed., Elsevier.
——, 1986: Internal waves, fossil turbulence, and composite ocean microstructure spectra. *J. Fluid Mech.*, **168**, 89–117.
——, 1987a: Oceanic turbulence: Big bangs and continuous creation. *J. Physicochem. Hydrodyn.*, **8**, 1–22.
——, 1987b: Fossil turbulence and intermittency in sampling oceanic mixing processes. *J. Geophys. Res.*, **92**, 5383–5404.
——, G. R. Stegen and S. O. McConnell, 1970: Measurements of the universal constant in Kolmogoroff's third hypothesis for high Reynolds number turbulence. *Phys. Fluids*, **13**, 2448–2451.
Gregg, M. C., 1976: Temperature and salinity microstructure in the Pacific equatorial undercurrent. *J. Geophys. Res.*, **81**, 1180–1196.
——, 1977: Variations in the intensity of small-scale mixing in the main thermocline. *J. Phys. Oceanogr.*, **7**, 436–454.
——, 1980: Microstructure patches in the thermocline. *J. Phys. Oceanogr.*, **10**, 915–943.
——, and M. G. Briscoe, 1979: Internal waves, finestructure, microstructure, and mixing in the ocean. *Rev. Geophys. Space Phys.*, **17**, 1524–1548.
——, and T. B. Meagher, 1980: The dynamic response of glass rod thermistors. *J. Geophys. Res.*, **85**, 2779–2786.
——, and A. M. Pederson, 1980: High resolution salinity measurement techniques. *Instruments and Methods in Air–Sea Interaction*, F. Dobson, L. Hasse and R. Davis, Eds., Plenum Press, 801 pp.
——, C. S. Cox and P. W. Hacker, 1973: Vertical microstructure measurements in the central North Pacific. *J. Phys. Oceanogr.*, **3**, 458–469.
Gurvich, A. S., and A. M. Yaglom, 1967: Breakdown of eddies and probability distributions for small-scale turbulence. *Phys. Fluids Suppl.*, **10**, S59–S65.
Hald, A., 1952: *Statistical Theory with Engineering Applications.* Wiley & Sons, 783 pp.
Hoel, P. G., S. C. Port and C. J. Stone, 1971: *Introduction to Probability Theory*, Houghton Mifflin, 258 pp.
Jenkins, W. J., 1980: Tritium and ^{3}He in the Sargasso sea. *J. Mar. Res.*, **38**, 533–569.
Kendall, M. G., and A. Stuart, 1967: *The Advanced Theory of Statistics.* Vol. 2, Hafner, 690 pp.
Kolmogoroff, A. N., 1941: The local structure of turbulence in incompressible viscous fluid for very large Reynolds numbers. *Dokl. Akad. Nauk, SSSR*, **30**, 301. *Turbulence—Classical Papers on Statistical Theory*, S. K. Friedlander and L. Topper, Eds., Interscience, 151–156.
——, 1962: A refinement of previous hypotheses concerning the local structure of turbulence in a viscous incompressible fluid at high Reynolds number. *J. Fluid Mech.*, **13**, 82–85.
Lange, R. E., 1981: Observations of near-surface oceanic velocity strain-rate variability during and after storm events. *J. Phys. Oceanogr.*, **11**, 1272–1279.
Munk, W. H., 1966: Abyssal recipes. *Deep-Sea Res.*, **13**, 707–730.
Oakey, N. S., 1982: Determination of the rate of dissipation of turbulent energy from simultaneous temperature and velocity shear microstructure measurements. *J. Phys. Oceanogr.*, **12**, 256–271.
——, 1985: Statistics of mixing parameters in the upper ocean during JASIN Phase 2. *J. Phys. Oceanogr.*, **15**, 1662–1675.
Osborn, T. R., 1978: Measurements of energy dissipation adjacent to an island. *J. Geophys. Res.*, **83**, 2939–2957.
——, and R. G. Lueck, 1985: Turbulence measurements with a submarine. *J. Phys. Oceanogr.*, **15**, 1502–1520.
Schedvin, J. C., 1979: Microscale temperature measurements in the upper ocean from a towed body. Ph.D. dissertation, University of California, San Diego, 422 pp.
Sichel, H. S., 1951: New methods in the statistical evaluation of mine sampling data. *Trans. Inst. Mining Metallurgy*, **61**, 261–288.
Tennekes, H., and J. C. Wyngaard, 1972: The intermittent small-scale structure of turbulence: Data processing hazards. *J. Fluid Mech.*, **55**, 93–103.
Washburn, L., and C. H. Gibson, 1982: Measurements of oceanic temperature microstructure using a small conductivity sensor. *J. Geophys. Res.*, **87**, 4230–4240.
——, and ——, 1984: Horizontal variability of temperature microstructure at the base of a mixed layer during MILE. *J. Geophys. Res.*, **89**, 3507–3522.
Williams, R. B., 1974: Direct measurements of turbulence in the Pacific equatorial undercurrent. Ph.D. dissertation, University of California at San Diego, SIO Rep. 74–19, 99 pp.
——, and C. H. Gibson, 1974: Direct measurements of turbulence in the Pacific equatorial undercurrent. *J. Phys. Oceanogr.*, **4**, 104–108.